An alternative replication niche for *Listeria monocytogenes* revealed by fluorescent tagging of bacterial secreted effectors

Caroline Peron Cane[1,2], Julien Leblanc[2], Laure Wingertsmann[2], José-Carlos Fernandez[2], Arnaud Gautier[3,4], Nicolas Desprat[1,2,5,*] and Alice Lebreton[2,6,*]

[1] Laboratoire de Physique de l'École normale supérieure, ENS, Université PSL, CNRS, Sorbonne Université, Université de Paris, 75005 Paris, France.

[2] Institut de biologie de l'ENS (IBENS), École normale supérieure, CNRS, INSERM, Université PSL, 75005 Paris, France.

[3] Sorbonne Université, École normale supérieure, Université PSL, CNRS, Laboratoire des Biomolécules, LBM, 75005 Paris, France.

[4] Institut Universitaire de France.

[5] UFR de Physique, Université Paris-Diderot, Université de Paris, 75005 Paris, France.

[6] INRAE, IBENS, 75005 Paris, France.

[*] Correspondence: alice.lebreton@ens.psl.eu; nicolas.desprat@phys.ens.fr

Abstract

Tracking the dynamics of secreted virulence factors in real time is impaired by the paucity of appropriate fluorescent tools. Here, we took advantage of the fluorogenic reporter FAST to tag secreted proteins and monitor infection dynamics among a population of epithelial cells infected by *Listeria monocytogenes* (*Lm*). Thereby, we unveiled the heterogeneity of *Lm* residence time in internalisation vacuoles. Although half of the bacterial population escaped rapidly, a significant fraction remained entrapped several hours in Long Residence Vacuoles (LRVs), independently of the secretion of the pore-forming toxin listeriolysin O (LLO). Unexpectedly, LLO enabled *Lm* to proliferate inside these compartments as fast as in the cytosol. LRVs display similarities with the spacious *Listeria*-containing phagosomes described in macrophages, and could constitute an alternative replication niche for *Lm* in epithelial cells.

Introduction

Bacterial pathogens harness distinct colonization strategies to take advantage of their host resources. While some remain extracellular, others adopt an intracellular lifestyle. Internalisation into host cells provides invasive bacteria with multiple abilities, such as that of crossing the organism barriers, escaping humoral immune surveillance, or disseminating throughout the organism as cargo of circulating cells. After internalisation, bacteria are entrapped inside primary vacuoles from where they can follow two distinct routes: either subverting endomembrane compartments, or leaving them. For instance, *Mycobacterium tuberculosis*, *Chlamydia trachomatis*, *Brucella abortus*, *Coxiella burnetii*, *Legionella pneumophila* perturb the maturation and rearrange the properties of vacuoles, thereby creating a compartment prone to their replication (Di Russo Case and Samuel, 2016; reviewed in Salcedo and Holden, 2005). Others, such as *Shigella flexneri* or *Listeria monocytogenes*, typically do not grow inside endomembrane compartments, but rather escape from entry vacuoles and gain access to the host cell cytoplasm, where they can replicate as well as exploit the host actin cytoskeleton for intracellular motility and cell-to-cell spread (reviewed in Gouin *et al*., 2005).

The foodborne pathogen *Listeria monocytogenes* (hereafter, *Lm*) is the causative agent of listeriosis, and has emerged as a model facultative intracellular bacterium (reviewed in Cossart and Lebreton, 2014; Radoshevich and Cossart, 2017). This pathogen can cross the protective barriers of its host and colonize tissues and organs by promoting its internalisation into non-phagocytic cells. The classical scheme of *Lm* intracellular life cycle implies that, both in professional phagocytes and in epithelial cells, *Lm* rapidly escapes from entry vacuoles due to the combined action of a potent pore-forming toxin, listeriolysin O (LLO), and of two phospholipases C (PlcA and PlcB), before replicating in the cytosol (Pizarro-Cerda and Cossart, 2018). All three genes (*hlyA* that encodes LLO, *plcA* and *plcB*) are part of *Lm* LIPI-I virulence gene cluster and are transcriptionally induced by PrfA, the main regulator of *Lm* virulence gene, in intracellular bacteria (reviewed in las Heras *et al*., 2011; Lebreton and Cossart, 2017).

LLO is a cholesterol-dependent pore-forming toxin (reviewed in Nguyen *et al*., 2018), secreted by *Lm* via the general secretion system (Sec). LLO assembles into oligomers on biological membranes, forming arcs and pores of several tens of nm that disrupt membrane integrity (Köster *et al*., 2014; Ruan *et al*., 2016). Its activity is optimal at acidic pH representative of the acidification occurring during the maturation of phagosomes (pH = 4.9 to 6.7) (Beauregard *et al*., 1997; Schuerch *et al*., 2005), which has been proposed to facilitate the escape of bacteria from entry vacuoles while avoiding damages to the host plasma membranes at neutral pH. Whereas LLO-deficient *Lm* cannot gain access to the host cytosol in many cell types, the activity of the phospholipases PlcA and PlcB and the influence of host factors render LLO dispensable for vacuole escape in several human epithelial cell lines (Burrack *et al*., 2009; Marquis *et al*., 1995). In phagocytes, it has been shown that bacteria secreting reduced amounts of LLO could remain entrapped in long-term compartments named Spacious *Listeria*-containing Phagosomes (SLAPs) and even replicate extremely slowly therein, with a doubling time in the range of 8 h (Birmingham *et al*., 2008).

The escape dynamics from the entry vacuole has been experimentally addressed using several distinct strategies. One of them consisted in using medium containing a membrane-impermeant fluorescent dye during infection (Beauregard *et al*., 1997; Myers *et al*., 2003). Upon encapsulation into the internalisation vacuoles together with invading bacteria, the fluorescent dye stained the intravacuolar space until it broke down. Alternative strategies were based on the assessment of vacuole rupture events and bacterial access to the host cytosol using fluorescent sensors. For instance, galectin-3 has been shown to label membrane remnants of damaged vacuoles and thereby allow the spotting of vacuole lysis (Paz *et al*., 2010). Likewise, actin or the Cell-wall Binding Domain CBD (a domain from the *Lm* phage endolysin Ply118) are recruited to the bacterial surface only once *Lm* has escaped the vacuole (Henry *et al*., 2006; Pizarro-Cerda and Cossart, 2018). Cytoplasmic FRET probes that are cleaved by a β-lactamase secreted by invasive bacteria have also been described as efficient reporters of vacuole rupture (Quereda *et al*., 2015; Ray *et al*., 2010). Even though these approaches yielded the order of magnitude of the time lapse between bacterial entry and vacuole escape in various cell types (between 15 min and 1 h), none of them has been used so far to determine the distribution of *Lm* residence time in entry vacuoles, which limits the interpretation of variations between conditions to that of average behaviours.

In order to measure the heterogeneity of *Lm* residence time in entry vacuoles and to assess the role played by LLO in the dynamics of bacterial escape from these compartments, we developed live imaging assays allowing an accurate measurement of the time elapsed between the moment when individual bacteria were internalised into cells, and the moment when the vacuole membrane was ruptured. We devised a strategy relying on the tagging of proteins secreted by bacteria with the FAST reporter system (Plamont *et al*., 2016). FAST is a 14-kDa protein tag which displays fluorescence upon binding with a synthetic fluorogenic probe supplied in the medium. The fluorogen is membrane permeant, non-toxic, and has very little fluorescence by itself. The small size of FAST, its fast folding kinetics, the reversible binding of fluorogens together with good brightness and photostability made this system an ideal candidate for tagging secreted proteins and imaging them in real time.

Using live imaging of FAST, we quantified the distribution of *Lm* residence times in primary vacuoles in the LoVo intestinal epithelial cell line. We observed that a fraction of the population of entry vacuoles lasted for several hours and were reminiscent of SLAPs. However, in contrast with SLAPs, these Long Residence Vacuoles (LRVs) were obtained in cells infected with wild type (WT) *Lm* as well as with a *hlyA* deletion strain. Furthermore, secretion of LLO inside LRVs allowed *Lm* to proliferate actively in these compartments, suggesting that besides its role in vacuole escape, LLO could contribute to set up an intravacuolar niche prone to *Lm* replication in epithelial cells.

Results

Fluorescent tagging with FAST of proteins secreted by *Listeria monocytogenes*

With the aim of detecting proteins that would be secreted by intracellular bacteria into their host cells in live-cell microscopy experiments, we explored the possibilities offered by the FAST reporter system for the fluorescent tagging of *Lm* secreted bacterial effectors. A set of integrative plasmids harbouring gene fusions under control of the P_{HYPER} promoter were designed (Figure 1A) and introduced in the genome of *Lm* strain LL195. These plasmids drove the constitutive production of either FAST or eGFP, either for intrabacterial localisation, or fused in their N-terminus to the secretion signal peptide (SP) of listeriolysin O (LLO) (SP-FAST and SP-eGFP constructs), or to full-length LLO (LLO-FAST, LLO-eGFP and untagged LLO constructs), a classical Sec substrate. A Myc tag in their C-terminus of all constructs allowed detection by immunoblotting. Protein production and secretion by each one of these seven strains was assessed by in-gel colloidal Coomassie staining and immunoblotting against the Myc tag, on bacterial total extracts and culture supernatant fractions from overnight-grown cultures in BHI (Figure S1). All transgenes were efficiently expressed by *Lm*, even though in varying amounts. As expected, constructs harbouring either the LLO SP, or full-length LLO, were recovered in bacterial culture supernatants, indicating that the SP of LLO promoted Sec-dependent export of FAST or FAST-tagged proteins, as well as eGFP-fusion proteins albeit to a lesser extent (Figure S1C, D). Constructs devoid of signal peptides were not detected in supernatant fractions, arguing against the release of proteins into the medium due to bacterial lysis. FAST-tagged Sec substrates can thus efficiently undergo secretion trough the general secretion pathway.

To assess whether the FAST reporter system remained fluorescent after secretion, we quantified the fluorescence signals in the culture medium of overnight-grown bacterial cultures in iLSM (Figure 1B). In presence of 5 μM of HBR-3,5DM, fluorescence was detected in the culture supernatant of strains secreting SP-FAST or LLO-FAST. Fluorescence intensities in the culture medium of strains producing non-secreted FAST or eGFP did not significantly differ from that of the strain producing untagged LLO, indicating that the release of fluorescent proteins in the culture medium was not due to bacterial lysis, and that FAST-labelled proteins retained their fluorescent properties after undergoing secretion trough Sec. By calibrating fluorescence measurements with a standard curve of known FAST:HBR-3,5DM concentrations diluted in the same minimal medium, we estimated the secreted concentration of tagged proteins; that of SP-FAST was 325±55 nM, and that of LLO-FAST around 28±6 nM.

Diverse attempts by others in Gram–negative bacteria (Dammeyer and Tinnefeld, 2012) and our own unpublished observations using tagged *Lm* virulence factors suggested that the Sec-dependent secretion and subsequent maturation of an eGFP tag into its active, fluorescent fold was inefficient. Surprisingly, the secretion of SP-eGFP—but not that of LLO-eGFP—gave rise to fluorescent signals in culture supernatants, even though in a range 10-fold lower than that obtained for the secretion of SP-FAST (Figure 1A).

A consistent proportion of eGFP undergoing Sec-dependent secretion was thus able to acquire its mature fold in bacterial culture medium, at least in iLSM, and when not fused to a bacterial effector.

Fluorescent tagging with FAST of *Shigella* effectors secreted through the type III secretion system

To evaluate the versatility of FAST as a reporter of bacterial secretion, we next asked if FAST was suitable for fluorescent tagging of effectors secreted through the syringe of the type III secretion system (T3SS) from a Gram-negative pathogen, *Shigella flexneri* (*Sf*) strain M90T. As model T3SS substrates, we tagged C-terminally with FAST-Myc the effectors OspF and IpaB (Figure 1C), which are translocated upon adhesion of *Sf* to host cells (reviewed in Pinaud *et al*., 2018). Bacterial total extracts and culture supernatant fractions were recovered from overnight-grown cultures in M9 medium, with or without stimulation of type-III dependent secretion by addition of Congo red. By immunoblotting these fractions against the Myc epitope, we observed that tagged OspF and IpaB were secreted into the bacterial culture medium upon Congo red induction (Figure S2A). The secretion of both tagged effectors was constitutive when using a Δ*ipaD* mutant strain for which translocation lacks gating controls (Ménard *et al*., 1994) (Figure S2B). We then assessed whether the fusion proteins secreted by the Δ*ipaD* strain had retained their fluorescent properties, by measuring fluorescence intensities in the supernatants of bacterial cultures grown overnight in M9 medium (Figure 1D). Fluorescence levels were consistently higher with this constitutively secreting strain than the fluorescence leakage measured for the WT strain when the T3SS was not induced. The concentration of OspF-FAST by the Δ*ipaD* strain was estimated to be 3.8 ± 0.3 nM, that of IpaB-FAST of 9.4 ± 1.7 nM. Like Sec substrates, FAST-tagged T3SS substrates can thus be translocated and keep fluorescent properties after secretion.

FAST-tagging of secreted *Listeria* effectors for live fluorescence microscopy

We next investigated whether the FAST reporter system was suited for intracellular detection in real-time microscopy of proteins secreted during infection. To this end, we monitored FAST signals in LoVo cells infected with *Lm* producing SP-FAST by confocal spinning disk microscopy over an infection time course (Figure 2, Movie S1). FAST fluorescence increased uniformly over time in the cytoplasm of infected cells (Figure 2A). At 562 nm—the emission wavelength specific for FAST:HBR-3,5DM—, fluorescent signals accumulated in cells infected with a strain producing SP-FAST, and not with a control isogenic strain that constitutively expressed mCherry (Figure 2B). In infected cells, fluorescence intensity—which corresponds to intracellular concentration of SP-FAST—increased exponentially over time (Figure 2C), likely mirroring the exponential growth of *Lm* in the host cytosol. After several hours of exponential increase, the intracellular fluorescence dropped suddenly, corresponding to the death of infected cells and the permeation of their membranes. The distribution of exponential increase rates in FAST fluorescence was indicative of the variability in the bacterial growth rates among infected cells (Figure 2D). The median rate was 0.66 h^{-1}, corresponding to a doubling time of 63 min. Consistently, a median bacterial growth rate of 0.72 h^{-1} (doubling

time of 58 min) was measured in similar conditions of infection and illumination by segmenting mCherry-labelled bacteria, and then measuring intrabacterial mCherry signals over time. The long tail of the distribution of exponential fluorescence increase rates likely reflected additional entries due to cell-to-cell spread from neighbouring cells. Altogether, the secretion of FAST into host cells allowed a quantitative monitoring of infection progression by live imaging of individual cells.

Residence time of *Listeria monocytogenes* in internalisation vacuoles

When FAST-tagged proteins were secreted into the large volume of the host cell cytoplasm, fluorescent signals were diluted and therefore only became visible after several hours of infection, once secreted FAST had accumulated sufficiently to be significantly discriminated from non-specific signals. Meanwhile, we reasoned that if *Lm* was confined inside micron-sized internalisation vacuoles, the higher concentration of secreted FAST molecules in a reduced volume would allow their detection and tracking until the rupture of vacuole membranes, thereby providing an accurate measurement of individual vacuole lifetimes (Figure 3A). Indeed, we observed that secreted FAST signals were enhanced in compartments that co-localized with mCherry-expressing bacteria within minutes after bacterial adhesion to cells, until these signals suddenly dropped when vacuoles ruptured (Figure 3B, Movie S2).

We used SP-FAST secretion to track intravacuolar fluorescent signals, and compare the residence time of WT or Δ*hlyA Lm* strains inside internalisation vacuoles formed in LoVo cells (Figure 3C-D). The *hlyA* deletion strain used in this experiment was generated by in-frame allelic replacement of the *hlyA* open reading frame with SP-FAST (Δ*hlyA*::SP-FAST, Figure S3A). The median value for the residence time of the WT strain was of 12.7±0.7 min (Figure 3D). When using the Δ*hlyA*::SP-FAST strain, the median residence time was significantly longer (21.1 ± 1.4 min) but remained of the same order of magnitude as for a strain producing LLO, confirming previous observations that *Lm* gained efficient access to the cytoplasm independently of LLO in epithelial cells (Burrack *et al*., 2009; Marquis *et al*., 1995). Unexpectedly, a large proportion of the entry vacuoles lasted for more than one hour (12.0 % for the WT strain; 14.8 % for the Δ*hlyA* mutant), and a consistent number of intact vacuoles was still observed 3 h p.i. (4.6 % for the WT strain; 6.2 % for the Δ*hlyA* mutant) (Figure 3C). The fact that the WT strain remained entrapped in Long Residence Vacuoles (LRVs) in proportions nearly identical to that of the Δ*hlyA* strain could either suggest that a sub-population of WT *Lm* failed to escape primary vacuoles in spite of LLO secretion, or that LLO was not produced by this sub-population of intravacuolar bacteria. To discriminate between these two hypotheses, we investigated whether LLO fused to a FAST tag was detected in vacuoles out of which *Lm* had failed to escape.

Long-term residence and rapid replication of *Listeria* inside LLO-decorated vacuoles

To examine whether LLO was produced and secreted by bacteria that remained entrapped in LRVs, we engineered a *Lm* strain where LLO was C-terminally fused with FAST at the endogenous *hlyA* locus (Figure S3A). In this strain, the fluorescence of FAST reported not only for LLO secretion and localisation,

but also for *hlyA* expression under its natural promoter. In order to be relevant for monitoring the dynamics of *Lm* intracellular infection, the 15-kDa FAST-Myc tag should not interfere with the function of the protein it reports for. We controlled that the haemolytic properties of the strain expressing *hlyA-FAST* did not differ from that of the WT strain (Figure S3B); the production, secretion and activity as a cytolysin of LLO are thus quantitatively and qualitatively preserved after C-terminal fusion with FAST.

The strain producing the LLO-FAST fusion also constitutively expressed mCherry, which allowed us to segment and track bacteria in 3D during infection. When imaging mCherry-labelled bacteria and LLO-FAST from 2 h post-infection (p.i.) in LoVo cells, we observed that *Lm* could remain entrapped inside LRVs for 9 h or more before the enclosed structure of LLO-labelled membranes eventually disrupted and bacteria dispersed into the cytosol (Figure 4A, Movie S3). Strikingly, the volume occupied by the mCherry signal increased over time, revealing that not only *Lm* inhabited LRVs for a long time, but that it was multiplying inside these compartments. The ability of *Lm* to grow inside LLO-FAST-labelled vacuoles was observed for both the LL195 genetic background (*Lm* lineage I, ST1) and the European *Lm* reference strain EGD-e (lineage II, ST9) (Figure S4A, Movie S4), indicating that this property was not specific to the hypervirulent clone LL195. Likewise, the proliferation of *Lm* inside LRVs was observed in Caco-2 cells, suggesting that LoVo cells were not the only epithelial niche allowing *Lm* to replicate inside endomembrane compartments (Figure S4B).

By tracking vacuoles and measuring their volumes over time, we determined the growth rate of WT *Lm* in LRVs. Intravacuolar growth was exponential, with a rate similar to that of free bacteria in the cytosol (Figure 4B, Figure S5A). The measured doubling time (90 min in this experimental setup; or down to 1 h when the intensity and frequency of illumination were reduced as in Figure 2D) was consistently shorter than that previously described in SLAPS, which was in the range of 8 h (Birmingham *et al*., 2008).

Role of listeriolysin O in the long-term intravacuolar residence and replication of *Listeria*

Our observations suggested that even when LRVs were permeated by LLO, their integrity was maintained and they allowed intravacuolar replication without rupturing. To further investigate whether LLO influenced *Lm* residence in LRVs, we took advantage of the LLO-FAST reporter strain in order to assess the variability in LLO abundance in these compartments. LLO-FAST signals measured in LRVs displayed a broad range of dynamics, indicating that LRV formation and preservation was independent of the amounts of secreted LLO (Figure S5B). In some LRVs, LLO-FAST accumulated linearly over time, while others displayed large-scale fluctuations in signals. Some LRVs yielded a strong signal while others displayed low levels of decoration by LLO. The lifetime of LRVs was correlated with neither the average concentration of LLO (Figure S5C) nor its maximal level (Figure S5D), suggesting that LLO concentration poorly influenced the probability of *Lm* escape from these structures.

Consistently with the absence of correlation between LLO abundance and bacterial escape from LRVs, not only WT and Δ*hlyA Lm* could reside in long-term vacuoles (Figure 3C, Figure 4C, Figure S3C), but LRVs were even observed when using a *prfA** mutant strain. This strain carries a *prfA* allele encoding a PrfA variant

with a G145S substitution that has been previously described to be constitutively active, and to lead to the strong overexpression of PrfA-dependent virulence genes, including that of *hlyA* (Ripio *et al*., 1997). Accordingly, the *in-vitro* haemolytic titre of the *prfA* strain we used was fifty-fold higher than that of the WT strain, indicative of LLO hyperproduction (Figure S3B). Highly elevated levels of secreted LLO thus did not impede the ability of *Lm* to reside and multiply inside LRVs for several hours. This feature is contrasting with that of SLAPs previously described to occur in phagocytes only when the expression of *hlyA* was moderate (Birmingham *et al*., 2008). Nevertheless, we observed by live-cell imaging that the very high levels of LLO secretion of the *prfA** strain hastened *Lm* escape from LRVs to a certain extent (Figure 4C, Figure S3C). In agreement with this result, the proportion of bacteria that replicated inside LRVs was lower when cells were infected with the *prf*A* strain than with the WT strain (Figure 4D), confirming that a major excess of LLO had a destabilising effect on the integrity of LRVs.

Although LLO was not necessary for LRV formation or *Lm* vacuole escape, we observed that the Δ*hlyA Lm* strain was unable to proliferate inside LRVs (Figure 4C, Figure S3C). Similar to SLAPs, LRVs thus required that bacteria secreted LLO to allow intravacuolar growth. Whereas the secretion of LLO was required for proliferation in LRVs, its quantity did not influence intravacuolar bacterial growth, since the *prfA** strain replicated at a similar rate as the WT strain in LRVs (Figure 4C). Consistently, the growth rate of LLO-FAST-secreting bacteria in LRVs was correlated with neither the average concentration (Figure S5E) nor the maximal level of LLO secretion (Figure S5F).

Origin and properties of *Listeria* long residence vacuoles in epithelial cells

The LRVs in which *Lm* replicated (Figure 4, Movies S3-4) likely originated from internalisation vacuoles from which bacteria had failed to escape (Figure 3C), unless they derived from secondary vacuoles produced by cell-to-cell spread, or by autophagy vacuoles where bacteria would have been entrapped after a first exposure to the cytoplasm. To assess whether the LRVs where *Lm* proliferated resulted from primary vacuoles, we monitored the intravacuolar stages of mCherry-expressing bacteria in LoVo cells transfected by the YFP-CBD fusion protein reporter (Henry *et al*., 2006). This reporter has been previously described to specifically label the surface of bacteria that have once been exposed to the host cytosol, because the cell wall-binding domain (CBD) from the *Lm* phage endolysin Ply118 binds the peptidoglycan of *Lm* with high affinity. Bacteria that replicated within LRVs remained unlabelled with YFP-CBD until the vacuole ruptured and bacteria dispersed throughout the cell (Figure 5A, Movie S5), indicating that they had not been in prior contact with the host cytosol. This result ruled out the possibility that bacteria became entrapped into secondary vacuoles by canonical autophagy or cell-to-cell spread after a first exposure to the host cell cytosol, and thereby confirmed that LRVs where *Lm* replicated originated from internalisation vacuoles.

Because the replication compartments we observed were reminiscent of SLAPs, we hypothesized that they could originate from a process analogous to LC3-associated phagocytosis (LAP), except it would occur in epithelial cells rather than in phagocytes. We thus endeavoured to further characterize this intravacuolar

replication niche, and analyse whether it had typical features of endosomal, lysosomal and/or noncanonical autophagy-derived compartments. By immunofluorescence staining of LoVo cells infected with mCherry-expressing *Lm* for 3 hours, we observed that the vacuoles containing several bacteria were negative for the early endosomal marker Rab5, while they were positive for the late endosomal marker Rab7, the lysosomal marker LAMP1, as well as LC3 (Figure 5B). These are typical markers of SLAPs, suggesting that, similar to what occurs in phagocytes, LC3 is lipidated and the noncanonical autophagy machinery recruited to the entry vacuole in epithelial cells. Also, as in SLAPs the pH inside LRVs remained neutral, as revealed by their absence of staining when using the acidophilic fluorescent probe LysoTracker Deep Red (Figure 5B). Altogether, we conclude that epithelial LRVs display molecular characteristics highly reminiscent of SLAPs, even though they allow a faster replication of *Lm*, and their maturation and rupture is less sensitive to the concentration of secreted LLO than the compartments observed in phagocytes.

Discussion

Exploring the dynamics of secreted virulence factors at the (sub-)cellular scale constitutes one of the main challenges for real-time microscopy of infectious processes. Here, we bring evidence that FAST offers a versatile, convenient opportunity for tackling this challenge. We took advantage of this system to measure the lifetime of *Lm* internalisation vacuoles, and to monitor the endomembrane localisation of the secreted *Lm* virulence factor LLO in live cells. As a result, we uncovered a new replicative niche for *Lm* in epithelial cells.

Real-time imaging of LLO during infection

On fixed samples, observing the localisation of LLO in infected cells has often constituted a hurdle, due to the poor quality of the labelling allowed by existing anti-LLO antibodies in immunofluorescence assays (*e.g.* Henry *et al.*, 2006). LLO localisation at vacuole membranes, or more recently in bacterial-derived membrane vesicles, was previously observed by electron microscopy using immunogold labelling (Coelho *et al.*, 2018; Quinn *et al.*, 1993). However, the precise dynamics of infectious processes cannot accurately be caught by fixed-cell studies. Besides, the high spatial resolution gained by electron microscopy compromises the observation of events at a cellular scale. As a complementary approach, LLO-eGFP fusions that were ectopically-expressed in host cells have enabled live imaging, yielding precious insight into the dynamics of LLO localisation at membranes and its turnover (Chen *et al.*, 2018). Nevertheless, ectopic expression by host cells cannot mimic the concentrations, location, and insertion into membranes from the inside of the vacuole obtained with bacterial secretion. Moreover, host cell signalling pathways and membrane dynamics differ between non-infected and infected cells. Here, we report that (*a*) the FAST system can be used to tag LLO without loss of function, (*b*) the LLO-FAST fusion, expressed from its endogenous promoter, is secreted by *Lm* in infected cells, (*c*) the vacuoles it decorates can be imaged with accuracy, and (*d*) some of these vacuoles unexpectedly last for several hours.

FAST, a versatile fluorescent reporter of bacterial secretion

Beyond the live detection of LLO secreted by *L. monocytogenes* through the general Sec secretion system, FAST opens new perspectives for real-time imaging of bacterial proteins secreted by a broader range of bacterial models and secretion systems. For instance, we provide evidence that FAST-tagged effectors are also efficiently secreted through the T3SS of *S. flexeri*.

In recent years, several strategies have emerged for fluorescent labelling of Sec– or T3SS– dependent substrates (reviewed in O'Boyle et al., 2018). Tagging bacterial effectors with Split-GFP provides a possible solution that has been successfully applied for live detection of *Salmonella* T3SS-dependent effectors or *Listeria* Sec-dependent secreted substrates (Batan *et al*., 2018; Van Engelenburg and Palmer, 2010); however, the reconstitution process is slow compared with microbial growth, and requires the stable expression of GFP1-10 in recipient cells, which limits its application in most biological systems. Superfolder GFP (sfGFP) or its derivative rsFolder have been successfully used for labelling *E. coli* periplasmic proteins exported through the Sec pathway (Dammeyer and Tinnefeld, 2012; Dinh and Bernhardt, 2011; Khatib *et al*., 2016; Peters *et al*., 2011), but to our knowledge has not been applied yet for other bacterial systems or in the context of host-pathogen interactions. Other fluorescent tags such as FlAsH and phiLOV were successfully used for monitoring the secretion of *Sf* T3SS-dependent effectors (Enninga *et al*., 2005; Gawthorne *et al*., 2016). Nevertheless, the toxicity in eukaryotic cells of the biarsenite dye used for FlAsH labelling and the rather modest brightness of phiLOV hamper their general use.

FAST compares with previously existing tools, while broadening the possible range of applications, due to (*a*) its ease of implementation (compared with Split-GFP); (*b*) its low toxicity (compared with FLASH); (*c*) its independence to oxygen allowing studies in anaerobes (Monmeyran *et al*., 2018; Streett *et al*., 2019) as well as (*d*) its rapid and reversible folding dynamics allowing transport through the T3SS (compared with GFP-derived probes); (*e*) its reasonable brightness and fast maturation time (compared with PhiLOV). In addition, by selecting the appropriate fluorogen, FAST-labelled proteins can be imaged at different wavelengths between 540 and 600 nm by selecting the appropriate fluorogen (Li *et al*., 2017), thereby providing users with flexibility in the choice of other fluorescent reporters in co-localisation studies. Red-shifted fluorogens also limit the toxicity of certain wavelength for bacteria when performing long-term imaging, and membrane-impermeant fluorogens offer the possibility to discriminate between intracellular and extracellular proteins (Li *et al*., 2018), for instance when addressing the localisation of bacterial effectors that anchor to the bacterial cell wall or to membranes.

Hence, FAST expands the panel of fluorescent reporters for monitoring secreted virulence factors and offers a wealth of opportunities to accurately seize the spatiotemporal aspects of infectious mechanisms.

LRVs, an alternative replication niche for *Listeria monocytogenes*

We document that in LoVo and Caco-2 epithelial cells, a consistent proportion of *Lm* fails to escape from internalisation vacuoles, but instead replicates efficiently inside LRVs, which are positively labelled by LLO-FAST (Figure 6). After several hours of intravacuolar residence and growth, the membrane of LRVs eventually rupture and bacteria resume a canonical cytosolic lifestyle.

The decoration of LRVs by LC3, Rab7 and LAMP1 as well as their neutral pH are reminiscent of the SLAPs previously described in phagocytes (Birmingham *et al*., 2008), and which derive from LAP (Mitchell *et al*., 2018). A process similar to LAP was also described to occur in epithelial cells during infection by *Sf* (Schille *et al*., 2017). Upon infection by *Lm*, we propose a model for the formation of replicative LRVs in epithelial cells, analogous to the current model of SLAP formation (Figure 6). The entrapment of *Lm* inside internalisation vacuoles could result in two distinct fates. (**A**) In the classically-described pathway, the coordinated actions of LLO, PlcA and PlcB result in a rapid disruption of the vacuole and escape of bacteria into the cytoplasm, where they can start replicating and polymerising actin. (**B**) In the second scenario, a proportion of internalisation vacuoles would undergo LC3 lipidation in addition to their maturation attested by decoration with Rab7, as well as fusion with lysosomes as suggested by LAMP1 labelling.

Whereas the LRVs that we observe in LoVo cells display similarities with SLAPs, they are notably distinct from LisCVs, an intravacuolar persistence niche of *Lm* recently described in human hepatocytes and trophoblast cells (Kortebi *et al*., 2017). Contrary to LRVs and SLAPs, LisCVs do not derive from primary vacuoles. Instead, they form late in the intracellular cycle of *Lm* by recapture of bacteria that have lost ActA-dependent motility. Indeed, bacteria found in LisCVs are labelled with YFP-CBD, while the bacteria we observe in LRVs are not. ActA function is indifferent to the formation of LRVs, since they are also observed when using a *prfA** strain, in which *actA* is constitutively expressed (Reniere *et al*., 2015). Moreover, whereas LRVs are lipidated by LC3, LisCVs are not. Last, *Lm* replicates in LRVs, whereas it adopts a viable, non-culturable state LisCVs and does not grow. Altogether, though occurring in epithelial cells, the features we describe for LRVs are consistent with compartments similar to SLAPs, and distinct from LisCVs. However, the replication of *Lm* inside LRVs is significantly faster than the 8 hours of doubling time reported in SLAPs (Birmingham *et al*., 2008), perhaps due to a lower bactericidal capacity of the epithelial niche compared with phagocytes. Membrane permeation by LLO might also attenuate the bactericidal properties of LRVs, and/or allow nutrient uptake through the permeated membrane, thereby promoting bacterial replication.

Together with LisCVs and SLAPs, LRVs enrich the palette of *Lm* intravacuolar lifestyles that can establish in various cells types. Apprehending the importance of LRVs in the context of *in vivo* infections prompts future investigation, as these compartments might provide shelter from cytosolic immune responses, or favour chronic forms of infections by dampening cell-to-cell spread within tissues. Deciphering the extent to which these intravacuolar niches influence the balance between bacterial fitness and host defences becomes critical to better appreciate long-term relationships between *Lm* and its host.

Material and methods

Bacterial strains, plasmids and culture conditions

The bacterial source strains used in this work were *Escherichia coli* NEB5α (New England Biolabs) for plasmid constructions, Rosetta(DE3)pLysS (Novagen) for recombinant protein production, the clinical isolate of *Listeria monocytogenes* LL195 (lineage I, ST1) (Weinmaier *et al*., 2013) for most of the experiments involving *Lm*, and *Shigella flexneri* M90T (Sansonetti *et al*., 1982) for experiments on *Sf* T3SS-dependent secretion. *Lm* reference strain EGD-e (lineage 2, ST9) (Glaser *et al*., 2001) (lineage II, ST9) was also used as a control that the observed LRVs were not specific to LL195. All strains were grown at 37°C under shaking at 190 rpm in Luria Bertani (LB) medium for *E. coli*, in LB or tryptic soy broth (TSB) for *Sf*, in brain hear infusion (BHI) or incomplete *Listeria* synthetic medium (Whiteley *et al*., 2017) for *Lm*. Whenever required, media were supplemented with antibiotics for plasmid selection (chloramphenicol, 35 µg/ml for *E. coli*; 20 µg/ml for *Sf*; 7 µg/ml for *Lm* or Ampicillin, 100 µg/ml), or Congo red (1 mg/ml) for activation of the *Sf* T3SS.

In order to favour the expression of transgenes, the DNA coding sequence for FAST, fused with a Myc-tag, was codon-optimized for *Lm* or *Sf* using the online Optimizer application (http://genomes.urv.es/OPTIMIZER/) in guided random mode. The optimized sequences (named gfAL001 and gfAL002, respectively) were obtained as synthetic Gene Fragments (Eurofins genomics) and will be provided upon request. The *Lm*-optimized sequence additionally contained the 5'-untranslated (5'-UTR) of the *hlyA* gene, and the sequence encoding the signal peptide (SP) of LLO in its N-terminal part.

For plasmid constructions in the pAD vector derived from the pPL2 backbone (Balestrino *et al*., 2010; Lauer *et al*., 2002), gfAL001 was amplified with primers oAL543-4, the sequence of the *Lm hlyA* gene encoding LLO was amplified from the EGD-e genomic DNA with primers oAL549-50b, and the coding sequence for eGFP was amplified from pAD-cGFP (BUG2479) (Balestrino *et al*., 2010) with primers oAL543-7. The UTR_{hlyA}-SP-FAST-Myc amplicon was inserted instead of UTR_{hlyA}-eGFP into the *Eag*I-*Sal*I restriction sites of pAD-cGFP, thus generating pAD-SP-FAST, where FAST is under control of the P_{HYPER} constitutive promoter (Figure 1A). pAD-FAST, pAD-eGFP, pAD-SP-eGFP, pAD-LLO, pAD-LLO-FAST and pAD-LLO-eGFP, all containing the 5'-UTR of *hlyA* and a Myc tag, were likewise generated by inserting the cognate DNA amplicons into the same restriction sites (Figure 1A). After cloning in *E. coli* NEB5α, these plasmids were integrated in the genome of *L. monocytogenes* strains LL195 at the $tRNA^{Arg}$ locus as previously described (Lauer *et al*., 2002).

For allelic replacement at the *hlyA* locus (Figure S3A), pMAD-Δ*hlyA*::FAST was created by amplifying three partially overlapping fragments by PCR: One thousand base pairs (bp) upstream (*plcA* gene) and downstream (*mpl* gene) of the *hlyA* open reading frame in the EGD-e genome were amplified, respectively, with oAL981-2 and oAL976-7, while the FAST-Myc open reading frame was amplified from pAD-FAST with

oAL983-75. These fragments were inserted into the pMAD vector (Trieu-Cuot *et al*., 1991), between the *Sal*I and *Bgl*II restriction sites by Gibson Assembly, using the NEBuilder HiFi DNA Assembly Cloning Kit (New England BioLabs). pMAD-*hly*A-FAST containing the last 1000 bp of *hlyA* fused with the FAST sequence, a Myc tag and one thousand bp downstream of *hlyA* was likewise generated by inserting the cognate DNA amplicons into the same restriction sites in pMAD. Allelic replacements of the *hlyA* open reading frame by these constructs in the genomes of *L. monocytogenes* strains LL195 and EGD-e were obtained as previously described (Trieu-Cuot *et al*., 1991). For complementation purposes in haemolysis assays, a simple in-frame deletion mutant of the *hlyA* gene was also created using the pMAD backbone.

For *Sf* constructs, *ipaB* and *ospF* were amplified from M90T genomic DNA with primers oAL703-4 and 707-8 respectively, and gfAL002 was amplified with primers oAL705-6. pSU2.1-OspF-FAST (Figure 1C) was obtained by inserting an oAL707-6 amplicon overlapping *ospF* and FAST-Myc, with a *Bam*HI restriction linker, in place of mCherry into the *Kpn*I-*Xba*I restriction sites of pSU2.1rp-mCherry (Campbell-Valois *et al*., 2015). pSU2.1-IpaB-FAST was generated by replacing *ospF* with *ipaB* (oAL703-4) at the *Kpn*I-*Bam*HI sites (Figure 1C). After cloning in *E. coli* NEB5α, these plasmids were introduced in *Sf* M90T by electroporation.

The complete lists of bacterial strains and oligonucleotides used in this work are supplied as Supplementary Tables S1 and S2, respectively.

Bacterial total extracts or secreted protein analysis

Bacterial total extracts or culture supernatants were recovered from 1 ml of *Lm* strains grown to an OD_{600nm} of 2.0 in BHI medium at 37°C as previously described (Lebreton *et al*., 2011).

Total bacterial extracts of *Sf* were prepared by boiling for 2 × 10 min at 95°C in 100 µl of Laemmli sample buffer (SB 1X) the bacterial pellets obtained by centrifugation of 1 ml of each strain grown to an OD_{600nm} of 2.0 in TCS medium at 37°C. For assessment of secretion leakage prior to T3SS induction, 2 ml of *Sf* culture supernatants were collected, precipitated with 16% trichloroacetic acid (TCA), and centrifuged for 30 min at 16,000 × *g* at 4°C. Protein pellets were washed twice in acetone before resuspension in 50 µl of SB 1X. For induction of secretion, *Sf* were resuspended in 0.6 ml phosphate buffered saline (PBS) containing 1 mg/ml of Congo red at a final OD_{600nm} of 40, and incubated at 37°C for 45 min. Bacteria were eliminated by centrifugation; 100 µl of supernatant were collected and mixed with 33 µl of SB 4X for SDS-PAGE separation. The remainder supernatant was TCA-precipitated and resuspended in 50 µl SB 1X as above.

10 µl of each sample were separated on 4-15% Mini-Protean TGX gels (Bio-Rad) by sodium dodecyl sulfate-polyacrylamide gel electrophoresis (SDS-PAGE). For immunoblots, after transfer on nitrocellulose membrane (Amersham) using PierceG2 Fast Blotter, proteins were probed with anti-Myc mouse monoclonal antibody #9E10 (sc-40, Santa Cruz Biotechnology) at a 1:400 dilution in PBS supplemented with 0.05% tween-20 and 5% skimmed milk powder, followed by secondary hybridization with anti-Mouse IgG-heavy and light chain Antibody (Bethyl) at a 1:50 000 dilution in the same buffer. Signals were detected using Pierce

ECL Plus Western Blotting Substrate and a Las4000 imager (GE Healthcare). Staining with colloidal Coomassie Brillant blue G-250 was performed as previously described (Neuhoff *et al*., 1988).

Haemolysis assay

The supernatants of overnight-grown cultures of *Lm* in BHI medium were recovered by centrifugation for 1 min at 6,000 × *g* followed by filtration through 0.2-µm pore filters, in order to eliminate bacteria. Serial two-fold dilutions of these supernatants were performed in round-bottom, clear, 96-well plates (100 µl final volume per well) using as a diluent PBS, the pH of which was adjusted to 5.6, and supplemented with 0.1% bovine serum albumin (BSA). Erythrocytes from defibrinated mice blood were washed twice in PBS pH 6.4 and diluted 1/10th in PBS pH 5.6. 50 µl of this suspension was added to each one of the wells containing diluted culture supernatants. After 30 min of incubation at 37°C, the plates were centrifuged for 10 min at 430 × *g* and haemolytic titres were calculated as the reciprocal of the dilution for which 50% of haemolysis was observed (Roche *et al*., 2001).

Fluorescence measurement on culture supernatants

Lm were grown overnight in BHI, washed and diluted to 1:10th in iLSM, and then grown for 6 h at 37°C, 180 rpm. Likewise, for secretion by *Sf* a culture in TSB was diluted to 1:10th in M9 medium supplemented with 0.2% glucose and 10 µg/ml nicotic acid. From 1 ml of culture, bacterial pellets were collected by centrifugation of the cultures at 6,000 × *g*, then washed in PBS and resuspended in 1 ml of PBS. The culture supernatants were filtered (0.2 µm pores). For fluorescence measurements of FAST-tagged fusions, 180 µl of each sample was mixed with 20 µl of 50 µM HBR-3,5DM ((*Z*)-5-(4-Hydroxy-3,5-dimethylbenzylidene)-2-thioxothiazolidin-4-one) to obtain a final concentration of 5 µM of fluorogen. 20 µl of PBS were used for negative controls, where no fluorescence was detected above that of the control medium (iLSM where *Lm* producing the non-fluorescent fusion LLO-Myc were grown, or supplemented M9 medium of a culture of *Sf* M90T Δ*ipaD*). Fluorescence intensity of technical triplicates was measured on a Spark 10M multimode microplate reader (Tecan), with excitation/emission wavelength set to 499/562 nm for FAST:HBR-3,5DM; 488/507nm for eGFP. After subtraction of background fluorescence corresponding to the negative control strains, fluorescence values in culture media were expressed as a percentage of the fluorescence measured for the suspension of bacteria expressing either non-secreted FAST, or eGFP (for *Lm*), or of M90T WT expressing OspF-FAST or IpaB-FAST (for *Sf*).

The standard curve for FAST fluorescence quantification was performed by diluting, in control medium, known amounts of recombinant FAST produced in *E. coli* Rosetta(DE3)pLysS as previously described (Plamont *et al*., 2016).

Each experiment was reproduced three times independently.

Infection and transfection of epithelial cells

Infections of intestinal epithelial cells were performed in the LoVo cell line originating from colon adenocarcinoma (ATCC Cat# CCL-229, RRID: CVCL_0399), grown in Ham's F-12K medium supplemented with 10% FBS, following ATCC recommendations. The Caco-2 epithelial cell line (ATCC Cat# HTB-37, RRID: CVCL_0025), also from colon adenocarcinoma, was used as a control that LRVs were not a specificity of LoVo cells. All cells were cultured at 37°C in a humidified atmosphere containing 5% CO_2. For live microscopy, cells were seeded on Ibidi µslides 72 h prior to infection at a density of 10^5 cells/ml, in 300 µg/ml of culture medium. When needed, cells were transfected 24 h before infection with pEYFP-C1-CBD expressing YFP-CBD (Henry *et al*., 2006), using Lipofectamine LTX (Invitrogen) and 1 µg/ml of plasmid, according to the manufacturer's specifications.

Lm strains were grown in BHI medium until they reached early stationary phase (OD_{600} of 2 to 3), washed in pre-warmed D-MEM, and then diluted in culture medium without serum to achieve a multiplicity of infection (MOI) of 5 (for long-term infections) to 30 (for short-term infections). Except for short-term imaging when bacterial entry was monitored under the microscope, after 30 min of bacteria-cell contact the inoculum was washed away by washing cells twice with serum-free medium containing 40 µg/ml of gentamicin, then the medium was replaced by complete culture medium without phenol red containing 25 µg/ml in order to kill extracellular bacteria.

Live fluorescence microscopy of infected cells

Cells infected as described above were observed in D-MEM without phenol red supplemented with 10% of FBS, 5 µM of HBR-3,5DM for fluorescence detection, 250 nM of the fluorogenic probe SiR-actin for actin detection, and 25 µg/ml of gentamicin for long-term infections. For experiments where early events were monitored, the labelling of actin by SiR-actin was initiated 2 h prior to infection by adding 250 nM of SiR-actin to the medium.

For live cell imaging, preparations were observed with a Nikon Ti PFS microscope coupled to a spinning disk confocal device (CSU-XI-A1, Yokogawa), connected to a cooled EM-CCD camera (Evolve, Photometrics), and equipped with a Cube for temperature control and a Brick gas mixed for a CO_2 and humidity control (Life Imaging Services). Image acquisition and microscope control were actuated with the MetaMorph software (Molecular Devices, RRID:SCR_002368). Fluorescent illumination was driven by three lasers, of wavelength 491 nm for eGFP, YFP of FAST, 561 nm for mCherry, and 635 nm for SiR-actin. Images were acquired with apochromat 63x objective lenses (NA 1.4) in 1 µm step-Z-stacks. Acquisition parameters were similar for all samples of an experiment. For snapshot display, maximum intensity signals from 16 successive stacks (*i.e*. 16 µm slices) were integrated with Fiji (RRID:SCR_002285). Each picture or video is representative of the population observed in three independent experiments.

For measurement of FAST accumulation in cells, images were first z-projected by maximum intensity, then fluorescence intensities were quantified on regions of fixed areas using Fiji. Vacuole tracking and bacterial growth rate calculations were performed using Matlab scripts (RRID:SCR_001622) tailored to each purpose as detailed below.

Tracking of primary vacuoles in short term infection assays

The slices of the z-stack obtained from spinning confocal imaging were projected onto a single plane (maximal projection). Fluorescent vacuoles were tracked using the plugin TrackMate in Fiji. The time at which tracks began during the infection was used to compute the time of *Lm* entry into LoVo cells. We then reconstructed the cumulative distribution of entries as a function of time and the entry rate was obtained by fitting the slope of the linear cumulative distribution of entries with time. Finally, the distribution of residence times in primary vacuoles was computed from the statistics of track length.

Tracking of LRVs in long-term infection assays

At 2 h p.i., Ibidi µslides were mounted on a confocal spinning disc microscope for observations. The mCherry signal labelling the bacterial cytoplasm was used to segment the volume of bacteria. Given the good signal-to-noise ratio of mCherry images, we performed a direct Otsu-thresholding algorithm on the mCherry stacks to obtain the 3D segmentation of bacteria. We then used MatLab routines to track objects based on their size and their location. To measure LLO-FAST signals in primary vacuoles, we applied on the FAST images the binary masks retrieved from mCherry segmentation and computed the average FAST signal in each mask. The fraction of the primary vacuoles into which *Lm* replicated was computed as the ratio of the number of tracked vacuoles that at least doubled their size during the course of the movie (12 h) to the initial number of bacteria. The growth rates of bacteria inside LRVs were computed by fitting the dynamics of segmented mCherry volumes to an exponential function.

Immunofluorescence or LysoTracker staining of infected cells

LoVo cells were seeded 48 h before infection in 24-well plates containing 12 mm diameter coverslips pre-coated with poly-L-lysine. Infection with bacteria expressing mCherry (for immunofluorescence experiments) or eGFP (for LysoTracker staining) was performed as described above, using a MOI of 30, except that plates were centrifuged for 1 min at 200 × *g* after addition of the inoculum in order to synchronise bacteria-cell contacts. 3 h p.i., cells were washed in pre-warmed PBS, fixed 20 min with 4% paraformaldehyde in PBS, then permeabilized for 5 min at room temperature with 0.5% Triton X-100 in PBS, and blocked for 5 min in PBS buffer containing 2% bovine serum albumin (BSA, Sigma). Incubation with primary antibodies in PBS buffer, 1 % BSA was performed for 1 h, followed by three PBS washes, and incubation with the Alexa Fluor 647-conjugated secondary anti-rabbit antibody (Molecular probes Cat# A21245, RRID:AB_141775, 2 µg/µl), Acti-stain 488 fluorescent phalloidin (Cytoskeleton #PHDG1, 70 nM) and DAPI (0.1 µg/µl) for 30 min. After

three additional washes, cover glasses were finally mounted on microscope slides with Fluoromount mounting medium (Interchim). Rabbit monoclonal primary antibodies from Cell Signalling Technologies against Rab5 (Cat #3547, RRID:AB_2300649), Rab7 (Cat# 9367, RRID:AB_1904103) and LAMP1 (Cat# 9367, RRID:AB_2687579) were used at a 1:200 dilution; rabbit polyclonal antibodies against LC3 (MBL International Cat# PM036, RRID:AB_2274121) were used at a 1:500 dilution.

Staining of acidic compartments was obtained by adding 50 nM of LysoTracker Deed Red (Molecular Probes #L12492) to the cell culture medium 1 h prior to observation. Infected cells were then observed in DMEM without phenol red, supplemented with 500 ng/ml Hoechst 33342 and 25 µg/ml gentamicin.

Preparations were observed with a Nikon Ti epifluorescence microscope (Nikon), connected to a digital CMOS camera (Orca Flash 4.0, Hamamatsu). Illumination was achieved using a SOLA-SE 365 source (Lumencor) and the following excitation/emission/dichroic filter sets (Semrock): DAPI or Hoechst, 377(50)/447(60)/FF409-Di03 ; Acti-Stain 488 or eGFP, 472(30)/520(35)/FF495-Di03 ; mCherry, 562(40)/632(22)/dic FF562-Di03; Alexa 647 or LysoTracker, 630(30)/684(24)/dic FF655-Di01. Images were acquired with Nikon apochromat 60x objective lenses (NA 1.4). Image acquisition and microscope control were actuated with the µManager software (RRID:SCR_016865), and processed with Fiji. Each picture is representative of the infected cell population.

Acknowledgements

We are grateful to Marie-Aude Plamont, Vinko Besic, Sebastian Rupp and Alison Tebo for their precious experimental assistance and eagerness to help solve technical issues. We thank Lionel Schiavolin and Didier Filopon for providing source strains and practical advice regarding *Sf* experiments. We thank the IBENS imaging facility for maintaining access to microscopy equipment that was instrumental to this work, and providing expert support whenever needed. We are indebted to the IBENS animal facility for kindly supplying the mice blood used in haemolysis assays. We thank Jost Enninga for unfailing proof of enthusiasm and insightful discussion.

Author contributions

AL, ND, AG designed the project. CPC, AL, ND, AG devised experiments and interpreted results. CPC, AL, ND, JL, LW, JCF performed experiments. CPC, ND analysed data. AL and ND wrote the manuscript with input from CPC and AG.

Funding

Work in the group of AL has received support under the program “Investissements d’Avenir” implemented by ANR (ANR-10-LABX-54 MemoLife and ANR-10-IDEX-0001-02 PSL University), Fondation pour la

Recherche Médicale (FRM-AJE20131128944), Inserm ATIP-Avenir and Mairie de Paris (programme Émergences – Recherche médicale). CPC received a doctoral fellowship from programme Interface pour le Vivant from Sorbonne University.

Declaration of interests

The authors declare the following competing financial interest: AG is co-founder and holds equity in Twinkle Bioscience/The Twinkle Factory, a company commercializing the FAST technology. FAST was patented by AG and L. Jullien (Patent Publication# WO/2016/001437, International Application# PCT/EP2015/065267).

References

Balestrino, D., Hamon, M.A., Dortet, L., Nahori, M.-A., Pizarro-Cerda, J., Alignani, D., Dussurget, O., Cossart, P., Toledo-Arana, A., 2010. Single-cell techniques using chromosomally tagged fluorescent bacteria to study *Listeria monocytogenes* infection processes. Appl Environ Microbiol 76, 3625–3636. doi:10.1128/AEM.02612-09

Batan, D., Braselmann, E., Minson, M., Nguyen, D.M.T., Cossart, P., Palmer, A.E., 2018. A multicolor split-fluorescent protein approach to visualize *Listeria* protein secretion in infection. Biophys. J. doi:10.1016/j.bpj.2018.03.016

Beauregard, K.E., Lee, K.D., Collier, R.J., Swanson, J.A., 1997. pH-dependent perforation of macrophage phagosomes by listeriolysin O from *Listeria monocytogenes*. J Exp Med 186, 1159–1163.

Birmingham, C.L., Canadien, V., Kaniuk, N.A., Steinberg, B.E., Higgins, D.E., Brumell, J.H., 2008. Listeriolysin O allows *Listeria monocytogenes* replication in macrophage vacuoles. Nature 451, 350–354. doi:10.1038/nature06479

Burrack, L.S., Harper, J.W., Higgins, D.E., 2009. Perturbation of vacuolar maturation promotes listeriolysin O-independent vacuolar escape during *Listeria monocytogenes* infection of human cells. Cell Microbiol 11, 1382–1398. doi:10.1111/j.1462-5822.2009.01338.x

Campbell-Valois, F.-X., Sachse, M., Sansonetti, P.J., Parsot, C., 2015. Escape of Actively Secreting *Shigella flexneri* from ATG8/LC3-Positive Vacuoles Formed during Cell-To-Cell Spread Is Facilitated by IcsB and VirA. MBio 6, e02567–14–14. doi:10.1128/mBio.02567-14

Chen, C., Nguyen, B.N., Mitchell, G., Margolis, S.R., Ma, D., Portnoy, D.A., 2018. The Listeriolysin O PEST-like Sequence Co-opts AP-2-Mediated Endocytosis to Prevent Plasma Membrane Damage during *Listeria Infection*. Cell Host Microbe 23, 786–795.e5. doi:10.1016/j.chom.2018.05.006

Coelho, C., Brown, L.C., Maryam, M., Vij, R., Smith, D.F., Burnet, M.C., Kyle, J.E., Heyman, H.M., Ramirez, J., Prados-Rosales, R., Lauvau, G., Nakayasu, E.S., Brady, N.R., Hamacher-Brady, A., Coppens, I., Casadevall, A., 2018. *Listeria monocytogenes* virulence factors, including Listeriolysin O, are secreted in biologically active extracellular vesicles. J Biol Chem jbc.RA118.006472. doi:10.1074/jbc.RA118.006472

Cossart, P., Lebreton, A., 2014. A trip in the "New Microbiology" with the bacterial pathogen *Listeria monocytogenes*. FEBS Lett 588, 2437–2445. doi:10.1016/j.febslet.2014.05.051

Dammeyer, T., Tinnefeld, P., 2012. Engineered fluorescent proteins illuminate the bacterial periplasm. Computational and Structural Biotechnology Journal 3, e201210013. doi:10.5936/csbj.201210013

Di Russo Case, E., Samuel, J.E., 2016. Contrasting Lifestyles Within the Host Cell. Microbiology Spectrum 4, 667–692. doi:10.1128/microbiolspec.VMBF-0014-2015

Dinh, T., Bernhardt, T.G., 2011. Using superfolder green fluorescent protein for periplasmic protein localization studies. J Bacteriol 193, 4984–4987. doi:10.1128/JB.00315-11

Enninga, J., Mounier, J., Sansonetti, P.J., Tran Van Nhieu, G., 2005. Secretion of type III effectors into host cells in real time. Nat Methods 2, 959–965. doi:10.1038/nmeth804

Gawthorne, J.A., Audry, L., McQuitty, C., Dean, P., Christie, J.M., Enninga, J., Roe, A.J., 2016. Visualizing the translocation and localization of bacterial type III effector proteins by using a genetically encoded reporter system. Appl Environ Microbiol 82, 2700–2708. doi:10.1128/AEM.03418-15

Glaser, P., Frangeul, L., Buchrieser, C., Rusniok, C., Amend, A., Baquero, F., Berche, P., Bloecker, H., Brandt, P., Chakraborty, T., Charbit, A., Chetouani, F., Couvé, E., de Daruvar, A., Dehoux, P., Domann, E., Domínguez-Bernal, G., Duchaud, E., Durant, L., Dussurget, O., Entian, K.D., Fsihi, H., García-del Portillo, F., Garrido, P., Gautier, L., Goebel, W., Gómez-López, N., Hain, T., Hauf, J., Jackson, D., Jones, L.M., Kaerst, U., Kreft, J., Kuhn, M., Kunst, F., Kurapkat, G., Madueno, E., Maitournam, A., Vicente, J.M., Ng, E., Nedjari, H., Nordsiek, G., Novella, S., de Pablos, B., Pérez-Diaz, J.C., Purcell, R., Remmel, B., Rose, M., Schlueter, T., Simoes, N., Tierrez, A., Vázquez-Boland, J.A., Voss, H., Wehland, J., Cossart, P., 2001. Comparative genomics of *Listeria* species. Science 294, 849–852. doi:10.1126/science.1063447

Gouin, E., Welch, M.D., Cossart, P., 2005. Actin-based motility of intracellular pathogens. Curr. Opin. Microbiol. 8, 35–45. doi:10.1016/j.mib.2004.12.013

Henry, R., Shaughnessy, L., Loessner, M.J., Alberti-Segui, C., Higgins, D.E., Swanson, J.A., 2006. Cytolysin-dependent delay of vacuole maturation in macrophages infected with *Listeria monocytogenes*. Cell Microbiol 8, 107–119. doi:10.1111/j.1462-5822.2005.00604.x

Khatib, El, M., Martins, A., Bourgeois, D., Colletier, J.-P., Adam, V., 2016. Rational design of ultrastable and reversibly photoswitchable fluorescent proteins for super-resolution imaging of the bacterial periplasm. Sci Rep 6, 92. doi:10.1038/srep18459

Kortebi, M., Milohanic, E., Mitchell, G., Péchoux, C., Prevost, M.-C., Cossart, P., Bierne, H., 2017. *Listeria monocytogenes* switches from dissemination to persistence by adopting a vacuolar lifestyle in epithelial cells. PLoS Pathog 13, e1006734. doi:10.1371/journal.ppat.1006734

Köster, S., van Pee, K., Hudel, M., Leustik, M., Rhinow, D., Kühlbrandt, W., Chakraborty, T., Yildiz, Ö., 2014. Crystal structure of listeriolysin O reveals molecular details of oligomerization and pore formation. Nat Commun 5, 3690. doi:10.1038/ncomms4690

las Heras, de, A., Cain, R.J., Bielecka, M.K., Vázquez-Boland, J.A., 2011. Regulation of *Listeria* virulence: PrfA master and commander. Curr. Opin. Microbiol. 14, 118–127. doi:10.1016/j.mib.2011.01.005

Lauer, P., Chow, M.Y.N., Loessner, M.J., Portnoy, D.A., Calendar, R., 2002. Construction, characterization, and use of two *Listeria monocytogenes* site-specific phage integration vectors. J Bacteriol 184, 4177–4186.

Lebreton, A., Cossart, P., 2017. RNA- and protein-mediated control of *Listeria monocytogenes* virulence gene expression. RNA biology 14, 460–470. doi:10.1080/15476286.2016.1189069

Lebreton, A., Lakisic, G., Job, V., Fritsch, L., Tham, T.N., Camejo, A., Matteï, P.-J., Regnault, B., Nahori, M.-A., Cabanes, D., Gautreau, A., Ait-Si-Ali, S., Dessen, A., Cossart, P., Bierne, H., 2011. A bacterial protein targets the BAHD1 chromatin complex to stimulate type III interferon response. Science 331, 1319–1321. doi:10.1126/science.1200120

Li, C., Mourton, A., Plamont, M.-A., Rodrigues, V., Aujard, I., Volovitch, M., Le Saux, T., Perez, F., Vriz, S., Jullien, L., Joliot, A., Gautier, A., 2018. Fluorogenic Probing of Membrane Protein Trafficking. Bioconjug. Chem. 29, 1823–1828. doi:10.1021/acs.bioconjchem.8b00180

Li, C., Plamont, M.-A., Sladitschek, H.L., Rodrigues, V., Aujard, I., Neveu, P., Le Saux, T., Jullien, L., Gautier, A., 2017. Dynamic multicolor protein labeling in living cells. Chem Sci 8, 5598–5605. doi:10.1039/c7sc01364g

Marquis, H., Doshi, V., Portnoy, D.A., 1995. The broad-range phospholipase C and a metalloprotease mediate listeriolysin O-independent escape of *Listeria monocytogenes* from a primary vacuole in human epithelial cells. Infect Immun 63, 4531–4534.

Ménard, R., Sansonetti, P.J., Parsot, C., 1994. The secretion of the *Shigella flexneri* Ipa invasins is activated by epithelial cells and controlled by IpaB and IpaD. EMBO J 13, 5293–5302.

Ménard, R., Sansonetti, P.J., Parsot, C., 1993. Nonpolar mutagenesis of the *ipa* genes defines IpaB, IpaC, and IpaD as effectors of *Shigella flexneri* entry into epithelial cells. J Bacteriol 175, 5899–5906.

Mitchell, G., Cheng, M.I., Chen, C., Nguyen, B.N., Whiteley, A.T., Kianian, S., Cox, J.S., Green, D.R., McDonald, K.L., Portnoy, D.A., 2018. *Listeria monocytogenes* triggers noncanonical autophagy upon

phagocytosis, but avoids subsequent growth-restricting xenophagy. Proc Natl Acad Sci USA 115, E210–E217. doi:10.1073/pnas.1716055115

Monmeyran, A., Thomen, P., Jonquière, H., Sureau, F., Li, C., Plamont, M.-A., Douarche, C., Casella, J.-F., Gautier, A., Henry, N., 2018. The inducible chemical-genetic fluorescent marker FAST outperforms classical fluorescent proteins in the quantitative reporting of bacterial biofilm dynamics. Sci Rep 8, 10336. doi:10.1038/s41598-018-28643-z

Myers, J.T., Tsang, A.W., Swanson, J.A., 2003. Localized reactive oxygen and nitrogen intermediates inhibit escape of *Listeria monocytogenes* from vacuoles in activated macrophages. The Journal of Immunology 171, 5447–5453. doi:10.4049/jimmunol.171.10.5447

Neuhoff, V., Arold, N., Taube, D., Ehrhardt, W., 1988. Improved staining of proteins in polyacrylamide gels including isoelectric focusing gels with clear background at nanogram sensitivity using Coomassie Brilliant Blue G-250 and R-250. Electrophoresis 9, 255–262. doi:10.1002/elps.1150090603

Nguyen, B.N., Peterson, B.N., Portnoy, D.A., 2018. Listeriolysin O: a phagosome-specific cytolysin revisited. Cell Microbiol e12988. doi:10.1111/cmi.12988

O'Boyle, N., Connolly, J.P.R., Roe, A.J., 2018. Tracking elusive cargo: Illuminating spatio-temporal Type 3 effector protein dynamics using reporters. Cell Microbiol 20, e12797. doi:10.1111/cmi.12797

Paz, I., Sachse, M., Dupont, N., Mounier, J., Cederfur, C., Enninga, J., Leffler, H., Poirier, F., Prevost, M.-C., Lafont, F., Sansonetti, P.J., 2010. Galectin-3, a marker for vacuole lysis by invasive pathogens. Cell Microbiol 12, 530–544. doi:10.1111/j.1462-5822.2009.01415.x

Peters, N.T., Dinh, T., Bernhardt, T.G., 2011. A fail-safe mechanism in the septal ring assembly pathway generated by the sequential recruitment of cell separation amidases and their activators. J Bacteriol 193, 4973–4983. doi:10.1128/JB.00316-11

Pinaud, L., Sansonetti, P.J., Phalipon, A., 2018. Host Cell Targeting by Enteropathogenic Bacteria T3SS Effectors. Trends Microbiol 26, 266–283. doi:10.1016/j.tim.2018.01.010

Pizarro-Cerda, J., Cossart, P., 2018. Listeria monocytogenes: cell biology of invasion and intracellular growth. Microbiology Spectrum 6. doi:10.1128/microbiolspec.GPP3-0013-2018

Plamont, M.-A., Billon-Denis, E., Maurin, S., Gauron, C., Pimenta, F.M., Specht, C.G., Shi, J., Quérard, J., Pan, B., Rossignol, J., Morellet, N., Volovitch, M., Lescop, E., Chen, Y., Triller, A., Vriz, S., Le Saux, T., Jullien, L., Gautier, A., 2016. Small fluorescence-activating and absorption-shifting tag for tunable protein imaging in vivo. Proc Natl Acad Sci USA 113, 497–502. doi:10.1073/pnas.1513094113

Quereda, J.J., Pizarro-Cerda, J., Balestrino, D., Bobard, A., Danckaert, A., Aulner, N., Shorte, S., Enninga, J., Cossart, P., 2015. A dual microscopy-based assay to assess *Listeria monocytogenes* cellular entry and vacuolar escape. Appl Environ Microbiol 82, 211–217. doi:10.1128/AEM.02302-15

Quinn, F., Pine, L., White, E., George, V., Gutekunst, K., Swaminathan, B., 1993. Immunogold labelling of *Listeria monocytogenes* virulence-related factors within Caco-2 cells. Res. Microbiol. 144, 597–608.

Radoshevich, L., Cossart, P., 2017. *Listeria monocytogenes*: towards a complete picture of its physiology and pathogenesis. Nat Rev Microbiol 16, 32–46. doi:10.1038/nrmicro.2017.126

Ray, K., Bobard, A., Danckaert, A., Paz-Haftel, I., Clair, C., Ehsani, S., Tang, C., Sansonetti, P.J., Van Nhieu, G.T., Enninga, J., 2010. Tracking the dynamic interplay between bacterial and host factors during pathogen-induced vacuole rupture in real time. Cell Microbiol 12, 545–556. doi:10.1111/j.1462-5822.2010.01428.x

Reniere, M.L., Whiteley, A.T., Hamilton, K.L., John, S.M., Lauer, P., Brennan, R.G., Portnoy, D.A., 2015. Glutathione activates virulence gene expression of an intracellular pathogen. Nature 517, 170–173. doi:10.1038/nature14029

Ripio, M.T., Domínguez-Bernal, G., Lara, M., Suárez, M., Vázquez-Boland, J.A., 1997. A Gly145Ser substitution in the transcriptional activator PrfA causes constitutive overexpression of virulence factors in *Listeria monocytogenes*. J Bacteriol 179, 1533–1540.

Roche, S.M., Velge, P., Bottreau, E., Durier, C., Marquet-van der Mee, N., Pardon, P., 2001. Assessment of the virulence of *Listeria monocytogenes*: agreement between a plaque-forming assay with HT-29 cells and infection of immunocompetent mice. Int. J. Food Microbiol. 68, 33–44.

Ruan, Y., Rezelj, S., Bedina Zavec, A., Anderluh, G., Scheuring, S., 2016. Listeriolysin O membrane damaging activity involves arc formation and lineaction — implication for *Listeria monocytogenes* escape from phagocytic vacuole. PLoS Pathog 12, e1005597. doi:10.1371/journal.ppat.1005597

Salcedo, S.P., Holden, D.W., 2005. Bacterial interactions with the eukaryotic secretory pathway. Curr. Opin. Microbiol. 8, 92–98. doi:10.1016/j.mib.2004.12.007

Sansonetti, P.J., Kopecko, D.J., Formal, S.B., 1982. Involvement of a plasmid in the invasive ability of *Shigella flexneri*. Infect Immun 35, 852–860.

Schille, S., Crauwels, P., Bohn, R., Bagola, K., Walther, P., van Zandbergen, G., 2017. LC3-associated phagocytosis in microbial pathogenesis. Int J Med Microbiol 308, 228–236. doi:10.1016/j.ijmm.2017.10.014

Schuerch, D.W., Wilson-Kubalek, E.M., Tweten, R.K., 2005. Molecular basis of listeriolysin O pH dependence. Proc Natl Acad Sci USA 102, 12537–12542. doi:10.1073/pnas.0500558102

Shen, A., Higgins, D.E., 2005. The 5' untranslated region-mediated enhancement of intracellular listeriolysin O production is required for *Listeria monocytogenes* pathogenicity. Mol Microbiol 57, 1460–1473. doi:10.1111/j.1365-2958.2005.04780.x

Streett, H.E., Kalis, K.M., Papoutsakis, E.T., 2019. A Strongly Fluorescing Anaerobic Reporter and Protein-Tagging System for Clostridium Organisms Based on the Fluorescence-Activating and Absorption-Shifting Tag Protein (FAST). Appl Environ Microbiol 85, 714. doi:10.1128/AEM.00622-19

Trieu-Cuot, P., Carlier, C., Poyart-Salmeron, C., Courvalin, P., 1991. Shuttle vectors containing a multiple cloning site and a lacZα gene for conjugal transfer of DNA from *Escherichia coli* to Gram-positive bacteria. Gene 102, 99–104. doi:10.1016/0378-1119(91)90546-N

Van Engelenburg, S.B., Palmer, A.E., 2010. Imaging type-III secretion reveals dynamics and spatial segregation of *Salmonella* effectors. Nat Methods 7, 325–330. doi:10.1038/nmeth.1437

Vincent, W.J.B., Freisinger, C.M., Lam, P.-Y., Huttenlocher, A., Sauer, J.-D., 2016. Macrophages mediate flagellin induced inflammasome activation and host defense in zebrafish. Cell Microbiol 18, 591–604. doi:10.1111/cmi.12536

Weinmaier, T., Riesing, M., Rattei, T., Bille, J., Arguedas-Villa, C., Stephan, R., Tasara, T., 2013. Complete genome sequence of *Listeria monocytogenes* LL195, a serotype 4b strain from the 1983-1987 listeriosis epidemic in Switzerland. Genome Announc 1, e00152–12–e00152–12. doi:10.1128/genomeA.00152-12

Whiteley, A.T., Garelis, N.E., Peterson, B.N., Choi, P.H., Tong, L., Woodward, J.J., Portnoy, D.A., 2017. c-di-AMP modulates *Listeria monocytogenes* central metabolism to regulate growth, antibiotic resistance and osmoregulation. Mol Microbiol 104, 212–233. doi:10.1111/mmi.13622

Figures

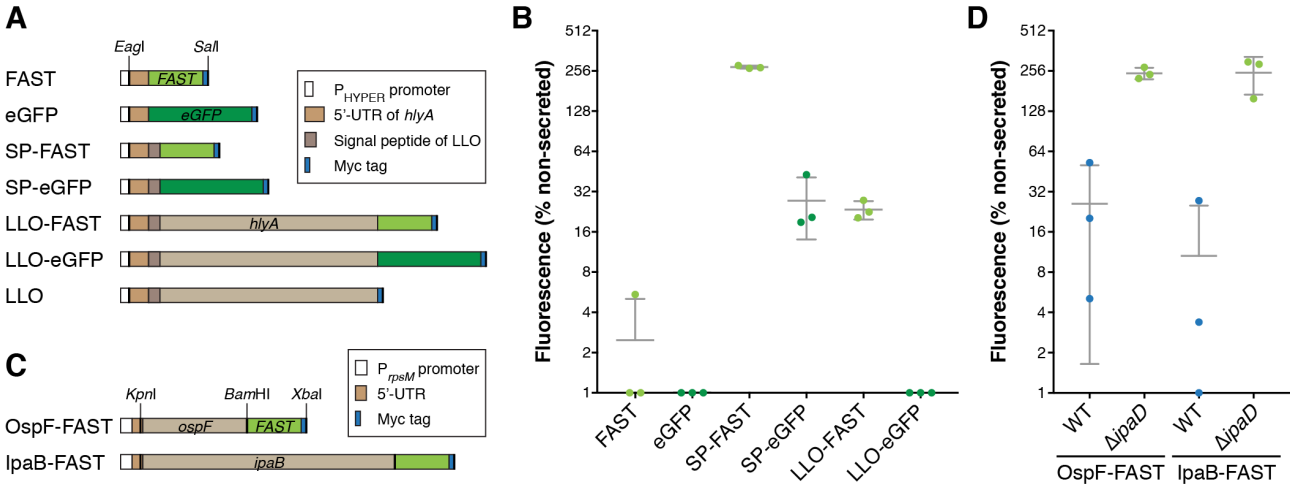

Figure 1. FAST-tagged proteins retain fluorescent properties after secretion into bacterial culture media.

(**A**) Diagram of constructs in the pAD vector for constitutive expression in *Listeria*.

(**B**) Fluorescent signals generated by proteins secreted by *Lm* in iLSM were measured in presence of 5 µM HBR-3,5DM. Intensities were expressed as a percentage of the fluorescence measured in a corresponding suspension of *Lm* producing non-secreted FAST or eGFP, taken as a reference.

(**C**) Diagram of constructs in the pSU2.1 vector for expression in *Shigella*.

(**D**) Fluorescent signals generated by proteins secreted by *Sf* in M9 medium were measured in presence of 5 µM HBR-3,5DM. Intensities were expressed as a percentage of the fluorescence measured in a corresponding suspension WT *Sf* producing OspF-FAST or IpaB-FAST, taken as a reference.

(**A, D**) All values below 1% of the reference were considered below the detection limit for this experiment, and represented as 1%. Normalized values, mean and standard deviations from three independent experiments were plotted.

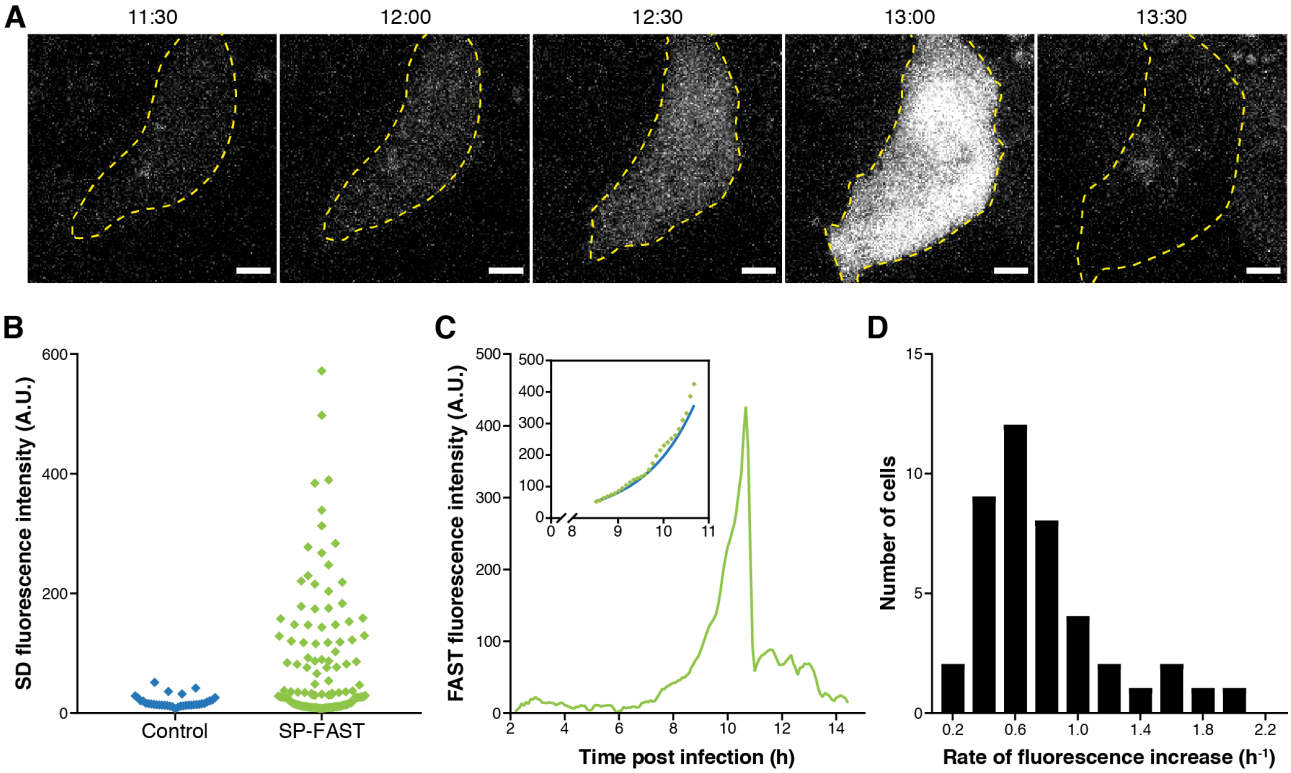

Figure 2. Secreted FAST accumulates exponentially in the cytoplasm of infected cells.

(**A**) Spinning-disk fluorescence microscopy images of LoVo cells infected with *Lm* expressing SP-FAST at different time-points post-infection. The cell contours were segmented based on SiR-actin staining, and are indicated with a dashed yellow line. Scale bar, 5 µm.

(**B**) Dispersion of fluorescence intensities. Fluorescence emission at 562 nm (FAST:HBR-3,5DM channel) was quantified over time within a region of fixed area in cells infected by *Lm* strains expressing either SP-FAST (in green, n=124) or mCherry as a negative control (in blue, n=35). As an indicator of the amplitude of fluorescence accumulation, the standard deviation of fluorescence intensity over time was plotted for each cell. A.U., arbitrary units.

(**C**) Intensity of FAST signals measured over time in a representative infected cell. Inset, exponential fit (in blue) obtained over the ascending part of the curve (in green dots).

(**D**) Distribution of the rates of increase of FAST fluorescence signals among the population of infected cells.

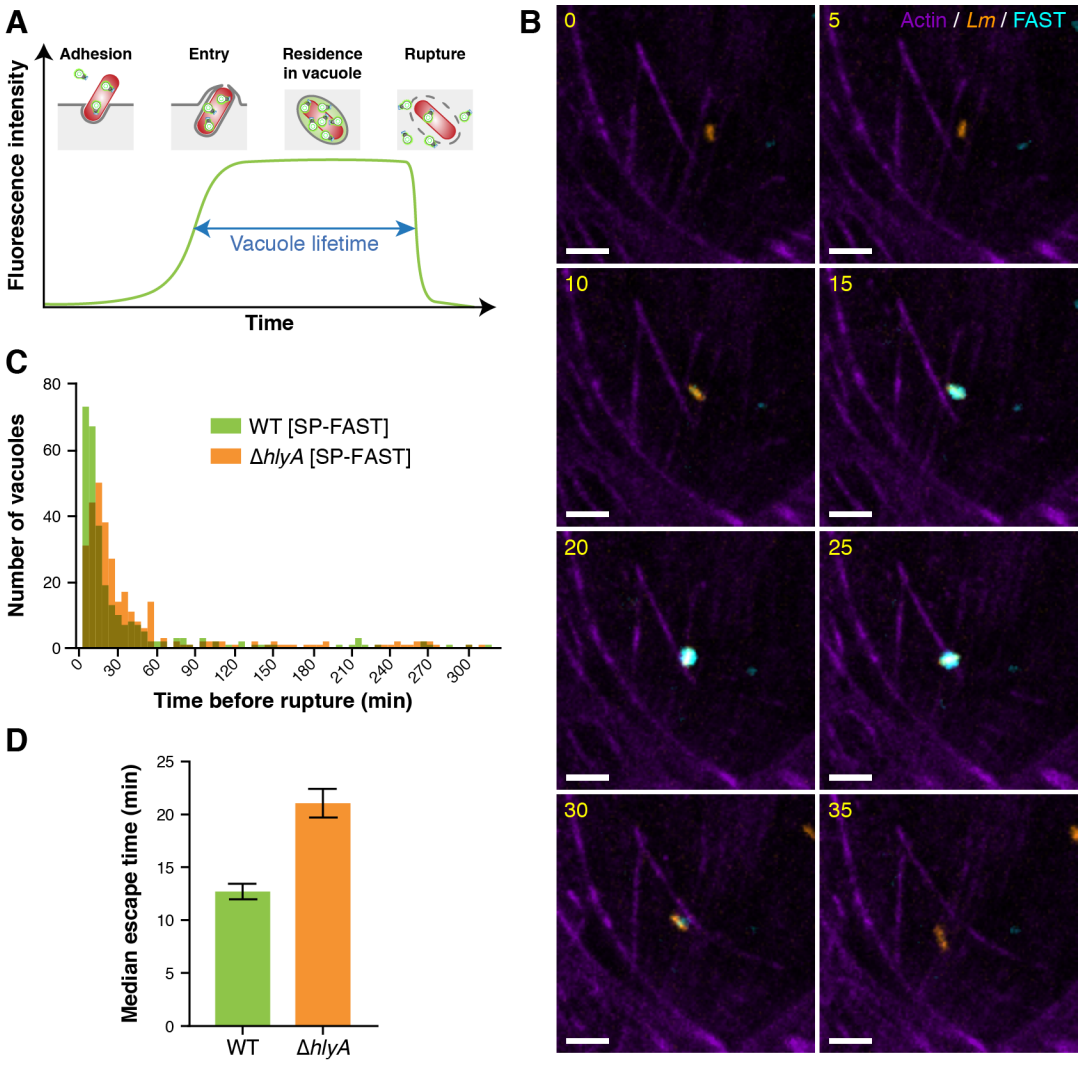

Figure 3. Secreted FAST reveals the heterogeneity of *Listeria* residence time in internalisation vacuoles.

(**A**) Expected profile of fluorescence accumulation in internalisation vacuoles for *Lm* secreting SP-FAST. After bacterial adhesion, *Lm* enters epithelial cells via a zipper mechanism. Secreted FAST should start accumulating in vacuoles upon their closure, and then remain visible until vacuole rupture. In each vacuole, a steady-state level of fluorescence might be temporarily reached, reflecting the equilibrium between bacterial secretion of FAST and its leakage in case of membrane permeation.

(**B**) Spinning-disk microscopy images of LoVo cells infected with *Lm ΔhlyA* expressing SP-FAST (cyan) and mCherry (orange) for 35 min after entry. The actin cytoskeleton (purple) was labelled with SiR-actin.

(**C**) Distribution of *Lm* residence times in internalisation vacuoles in LoVo cells. Green, WT strain carrying an integrated pPL2-SP-FAST plasmid (n=284); Orange, *ΔhlyA*::SP-FAST strain carrying an integrated pHpPL3-mCherry plasmid (n=306).

(**D**) Median half-lives of SP-FAST-labelled vacuoles calculated from the distribution displayed in (C).

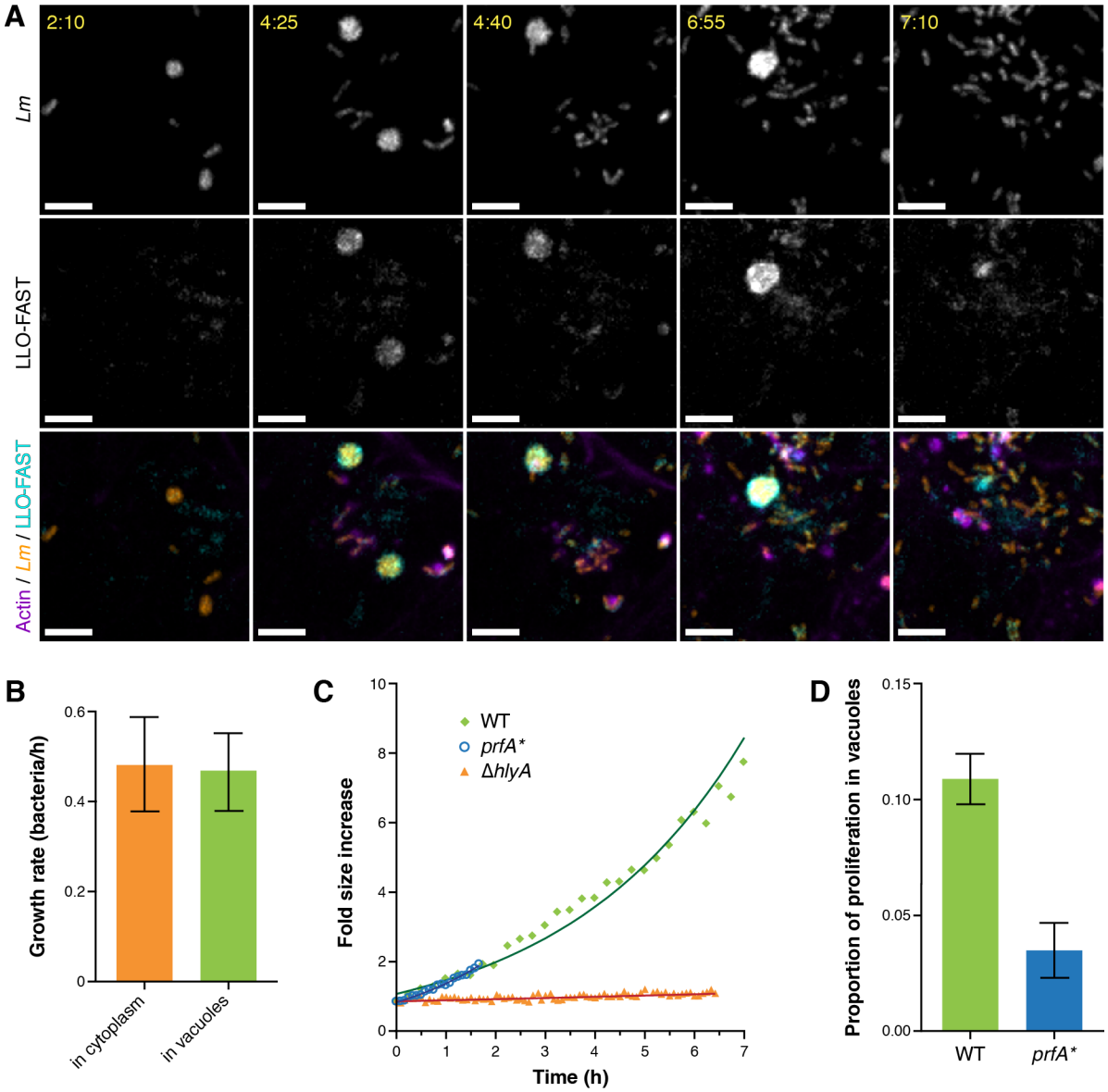

Figure 4. ***Listeria monocytogenes*** **replicates inside long-term vacuoles decorated with LLO.**

(**A**) Spinning-disk microscopy images of LoVo cells infected with *Lm* expressing both LLO-FAST (in cyan) and mCherry (in orange) at several time-points post-infection. SiR-actin staining is shown in purple. Scale bar, 5 µm.

(**B**) Growth rates of *Lm* expressing mCherry in the cytoplasm (orange, n=3) or in LRVs (green, n=7) in infected LoVo cells.

(**C**) Quantification of the increase in volume of LRVs, and thus of the growth of the bacteria they contain, for the WT (green), the *prfA** (blue) or the *ΔhlyA* (orange) *Lm* strains in infected LoVo cells.

(**D**) Proportion of intracellular *Lm* that, starting from 2 h p.i., proliferated inside LVRs during the subsequent time-course of 12 h. Green, WT strain (n=193); blue, *prfA** strain (n=57).

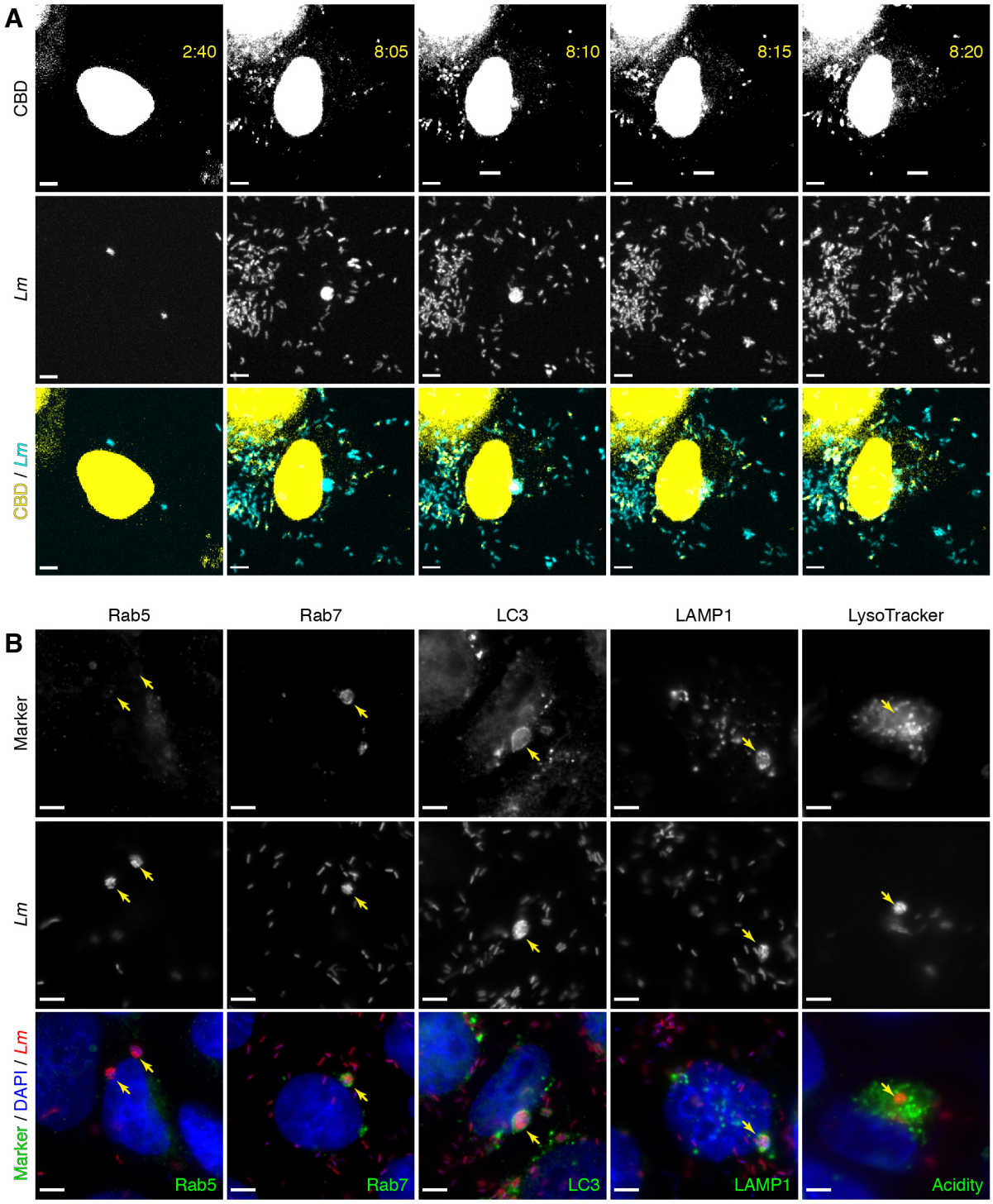

Figure 5. *Listeria* epithelial LRVs derive from internalisation vacuoles and display typical markers of LC3-associated phagocytosis.

(**A**) Differential labelling by CBD-YFP of the cytosolic *versus* intravacuolar populations of intracellular bacteria. LoVo cells were transfected with pEYFP-CBD (in yellow) 24 h before being infected with *Lm* expressing mCherry (in cyan), then imaged at different time-points post infection.

(**B**) Rab5, Rab7, LC3 and LAMP1 (in green) were detected by immunofluorescence in LoVo cells infected for 3 h with mCherry-expressing bacteria (in red). For acidity staining, LoVo cells infected for 2 h with eGFP-expressing bacteria (in red) were stained with LysoTracker Deep Red (in green), and observed 1 h afterwards. Observations were performed on an inverted spinning disk microscope. Scale bars, 5 μm.

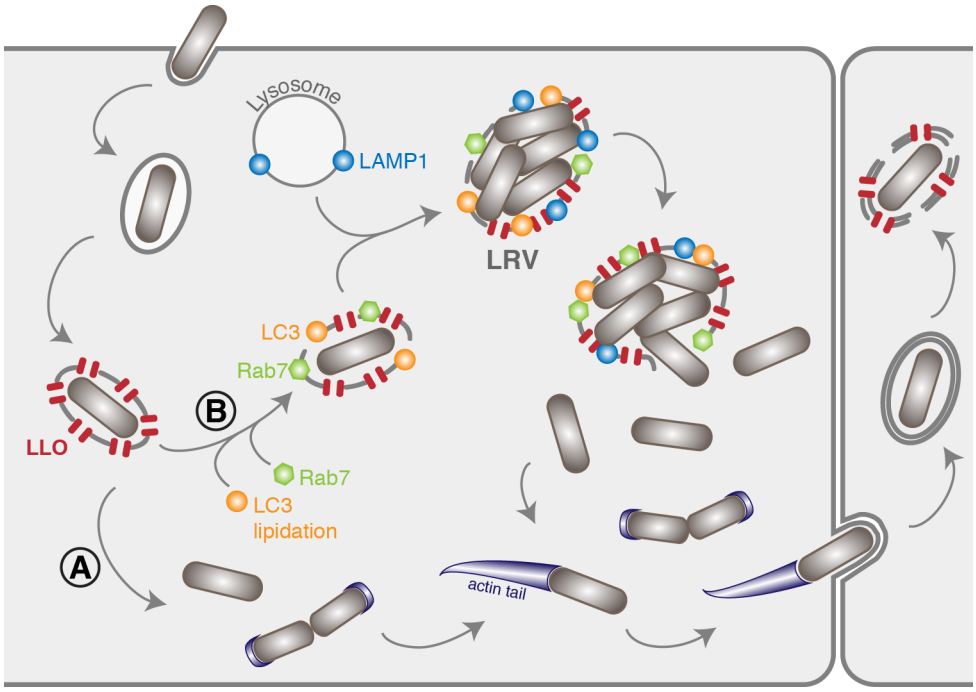

Figure 6. Extended model of the intracellular life cycle of *Listeria monocytogenes* in colon adenocarcinoma epithelial cell lines.

(**A**) In the classical scenario, after receptor-mediated entry, *Lm* evades the vacuole thanks to the combined action of LLO and phospholipases.

(**B**) Here we identified a population of *Lm* that can remain for several hours and multiply inside LRVs. These compartments are neutral, positive for Rab7, LC3 and LAMP1, and decorated with LLO. This second population finally escapes into the cytoplasm at later time points.

Supplementary materials

Supplementary materials include Movies S1 to S5, Figures S1 to S5 and Tables S1 to S2.

Movies

Movie S1. Accumulation of secreted FAST in the cytoplasm of infected cells.

LoVo cells infected with *Lm* expressing SP-FAST were observed between 2 and 14 h post-infection by spinning-disk microscopy. Scale bar, 10 µm.

Movie S2. Observation of secreted FAST signals in *Listeria* entry vacuoles.

LoVo cells infected with *Lm* expressing mCherry (**A**) or mCherry and SP-FAST (**B**) were observed between 0 and 3.25 h post-infection by spinning-disk microscopy. Green, FAST channel (non-specific signals in (A); secreted FAST in **B**); red, mCherry channel; blue, SiR-actin channel. Tracks for individual internalisation vacuoles containing mCherry-bacteria and SP-FAST are displayed in yellow. Scale bar, 10 µm.

Movie S3. Observation of the decoration of LRVs by LLO-FAST in *Listeria* cells infected by *Lm* LL195.

LoVo cells infected with *Lm* LL195 expressing both mCherry and LLO-FAST were observed between 2 and 8 h post-infection by spinning disk microscopy. Orange, FAST channel; cyan, mCherry channel; purple, SiR-actin channel. Scale bar, 5 µm.

Movie S4. Observation of the decoration of LRVs by LLO-FAST in *Listeria* cells infected by *Lm* EGD-e.

LoVo cells infected with *Lm* EGD-e expressing both mCherry and LLO-FAST were observed between 2 and 9 h post-infection by spinning disk microscopy. Orange, FAST channel; cyan, mCherry channel; purple, SiR-actin channel. Scale bar, 5 µm.

Movie S5. Imaging of the differential labelling by CBD-YFP of the cytosolic *versus* intravacuolar populations of intracellular bacteria.

LoVo cells were transfected with pEYFP-CBD 24 h being infected with *Lm* expressing mCherry, then imaged by spinning disk microscopy from 2 to 8 h p.i. Yellow, CBD-YFP channel; cyan, mCherry channel. Scale bar, 5 µm.

Supplementary Figures

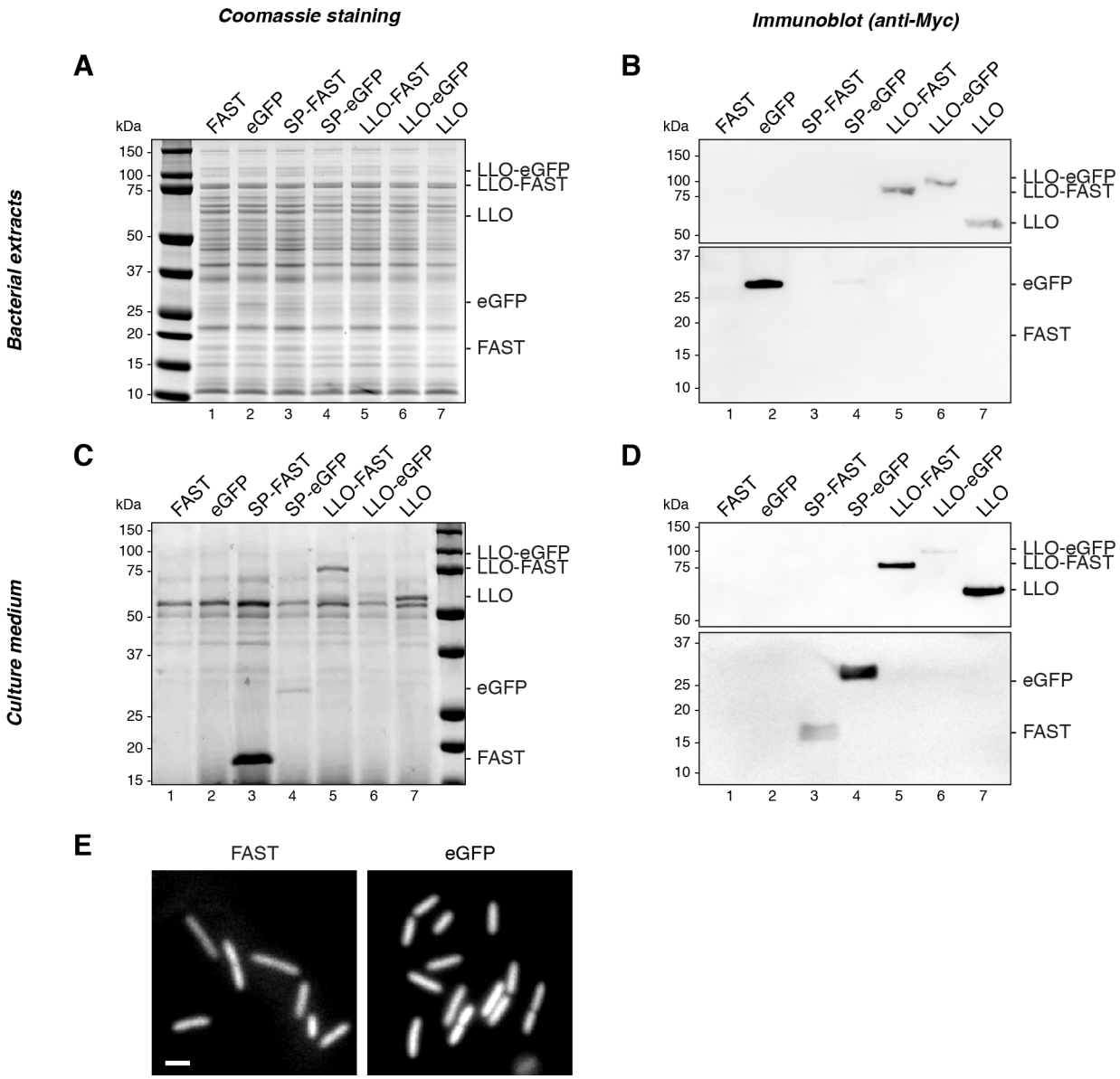

Figure S1. Production and secretion of the Myc-tagged fusion proteins by *Listeria monocytogenes* LL195 (constitutive expression from an integrated pAD vector).

Protein production and secretion of Myc-tagged fusion proteins was assessed by colloidal Coomassie staining (**A**, **C**) and immunoblotting with anti-Myc antibodies (**B**, **D**) of bacterial total extracts (**A**, **B**) and culture supernatant fractions (**C**, **D**) from overnight-grown cultures in BHI, separated by SDS-PAGE. (**E**) Epifluorescence microscopy observation of strains producing non-secreted FAST or eGFP. Scale bar, 2 µm.

Most Myc-tagged protein constructs were detected by immunoblotting in the corresponding bacterial pellet fraction, indicating that transgenes were expressed, even though in varying amounts (**B**, lanes 2, 4-7).

Constructs harbouring the LLO SP or full-length LLO were recovered in bacterial supernatants (**C**, **D**, lanes 3-7), suggesting that the SP of LLO promoted Sec-dependent export of not only of FAST or FAST-tagged proteins, but also of eGFP-fusion proteins. The secretion of eGFP-tagged proteins seemed less efficient than that of FAST-tagged protein (**C**, compare lane 3 with 4; **D**, compare lane 5 with 6), consistent with previous reports that eGFP is a poor substrate for Sec-dependent secretion (Dammeyer and Tinnefeld, 2012). Constructs devoid of signal peptides were not detected in supernatant fractions (**C**, **D**, lanes 1-2), arguing against the release of proteins into the culture medium due to bacterial lysis.

For technical reasons likely due to the small size of FAST-Myc (15 kDa), it was not or barely detected by immunoblotting (**B**, **D**, lanes 1, 3); nevertheless, a strong signal corresponding to this polypeptide was visible on Coomassie-stained gels of the supernatant fractions, attesting of its secretion (**C**, lane 3). For bacterial pellet fractions (**A**, lanes 1, 3), signal from other proteins masked possible bands from that polypeptide; however, observation in microscopy (**E**) confirmed the non-secreted form of FAST was also produced.

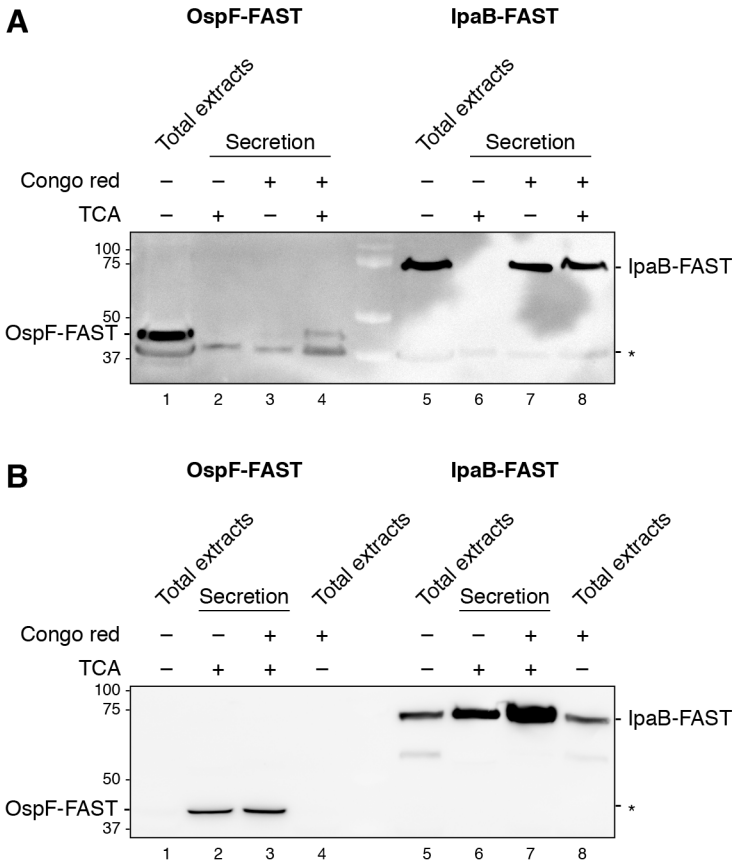

Figure S2. Production and secretion of the Myc-tagged fusion proteins by *Shigella flexneri* M90T (constitutive expression from a pSU2.1rp vector).

Protein production and secretion of Myc-tagged fusion proteins was assessed by immunoblotting with anti-Myc antibodies of bacterial total extracts culture supernatant fractions, with or without induction of secretion by the T3SS using Congo red, and with or without TCA precipitation in order to concentrate samples. (**A**) Samples from wild type M90T *Shigella flexneri*. (**B**) Samples from M90T Δ*ipaD*, in which T3SS secretion is constitutive. *, non-specific band.

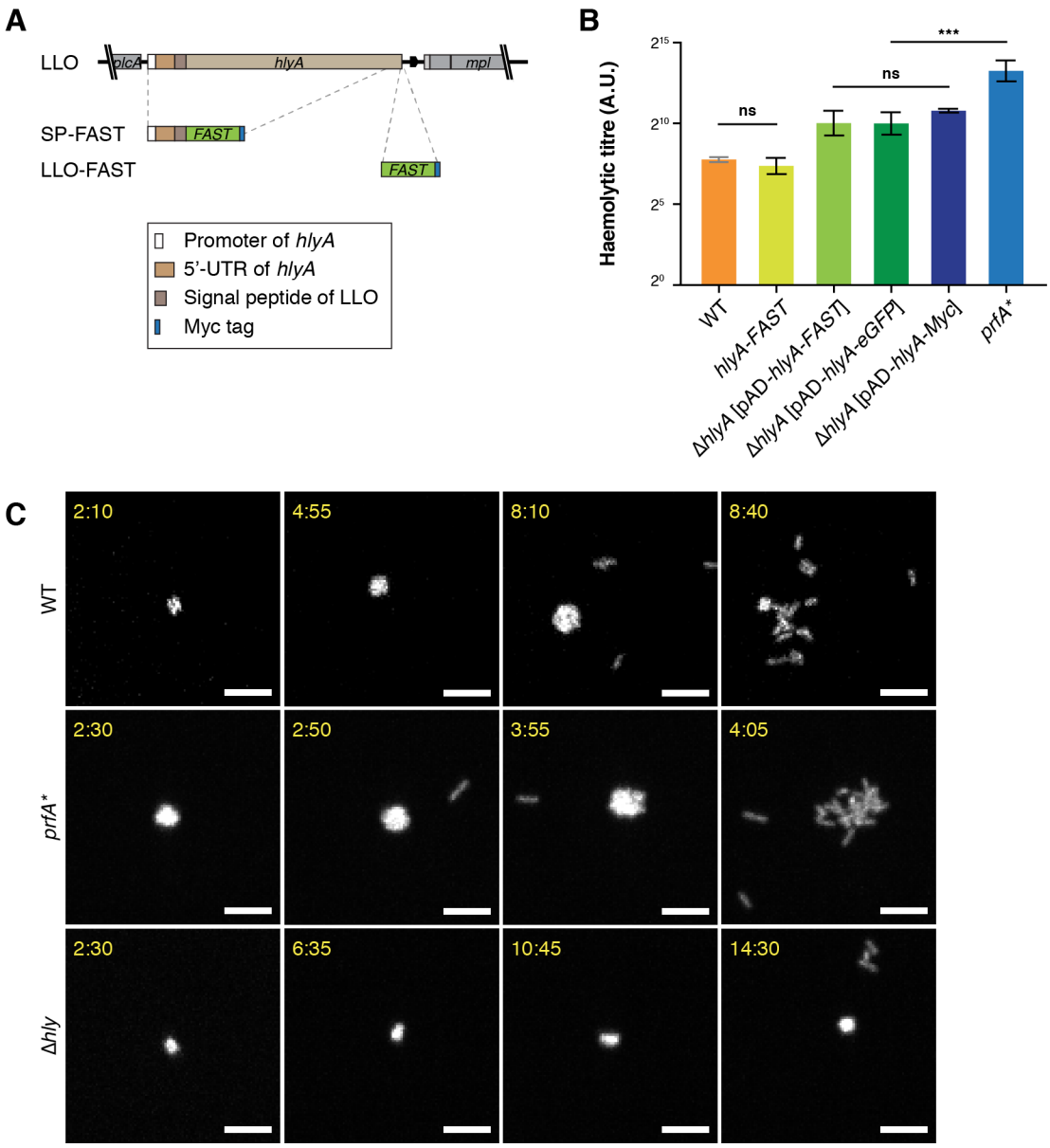

Figure S3. Construction, haemolytic properties and intravacuolar growth of various *Listeria monocytogenes* strains used in this study.

(**A**) Diagram of allelic replacement of the *hlyA* locus by a cassette expressing SP-FAST under the endogenous *hlyA* promoter, and of C-terminal tagging of LLO with FAST by in-frame fusion.

(**B**) Haemolytic properties of the *Listeria monocytogenes* strains producing FAST– or eGFP–tagged fusion LLO used in this study. The haemolytic titre measured for the strain where LLO was C-terminally tagged with FAST-Myc at the *hlyA* locus (*hlyA-FAST*) did not differ from that of the WT *Lm* strain. Haemolytic titres were enhanced for Δ*hlyA* deletion strains that had been complemented by *hlyA* fusion genes under control of the strong, constitutive P_{HYPER} promoter in the pAD vector. Fusion with FAST-Myc or eGFP-Myc did not affect haemolytic properties, compared to a simple fusion with Myc. None of these strains reached the intense haemolytic properties of the *prfA** strain, where the expression of *Lm* virulence genes (including *hlyA*) is

deregulated, due to the constitutive activity of the transcriptional activator PrfA (Ripio *et al*., 1997). The haemolytic titre of the Δ*hlyA* strain being null, it was not represented on this graph. ANOVA was used for statistical testing. ns, non-significant; ***, $p < 0.001$.

(**C**) Time-course of replication of mCherry-expressing *Lm* inside a LRV for the WT, the *prfA** and the Δ*hlyA* strains during the infection of LoVo cells. Scale bar, 5 μm.

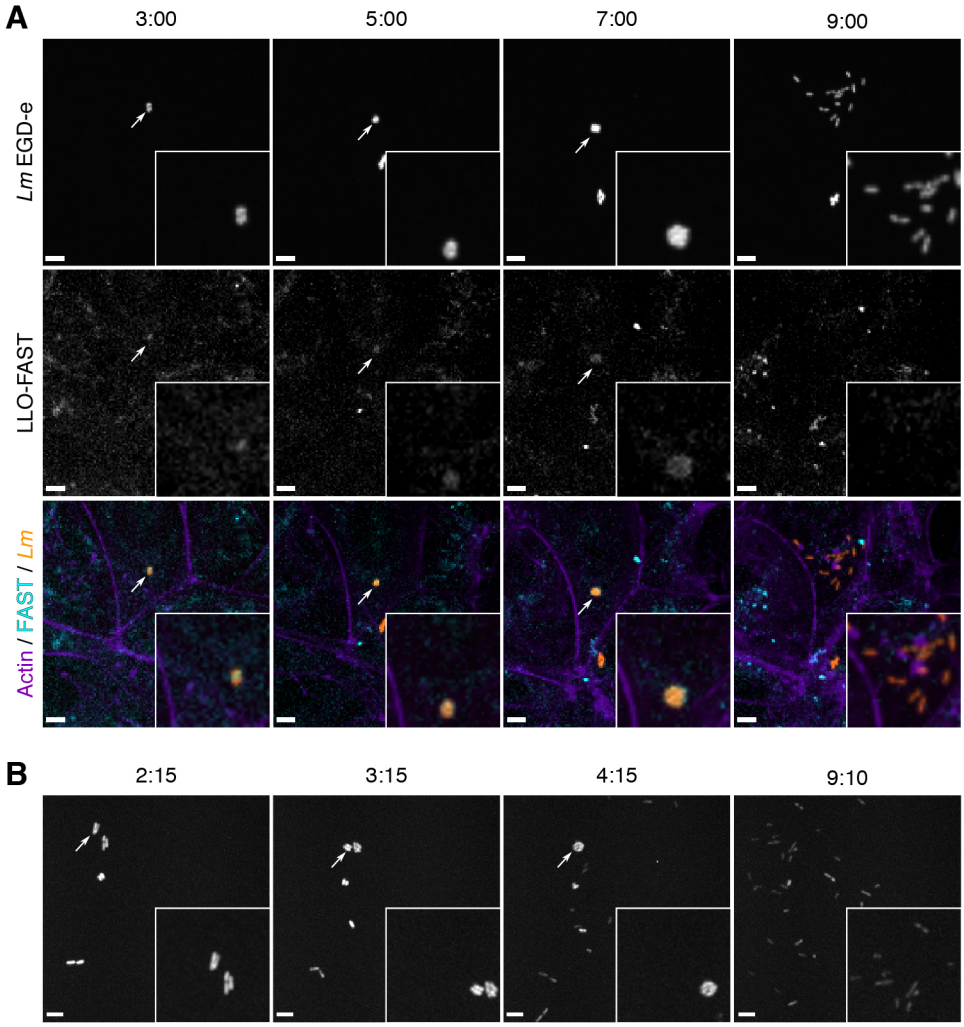

Figure S4. Proliferation of *Lm* inside LRVs is also observed when using the EGD-e strain in LoVo cells, or the LL195 strain in Caco-2 cells.

(**A**) LoVo cells infected with *Lm* EGD-e expressing both mCherry and LLO-FAST were observed between 2 and 8 h post-infection by spinning disk microscopy. On the merged image, LLO-FAST is in cyan, mCherry is in orange, and SiR-actin is in purple. Scale bar, 5 µm.

(**B**) Time-course of replication of mCherry-expressing *Lm* LL195 inside a LRV, observed in the Caco-2 cell line. Scale bar, 5 µm.

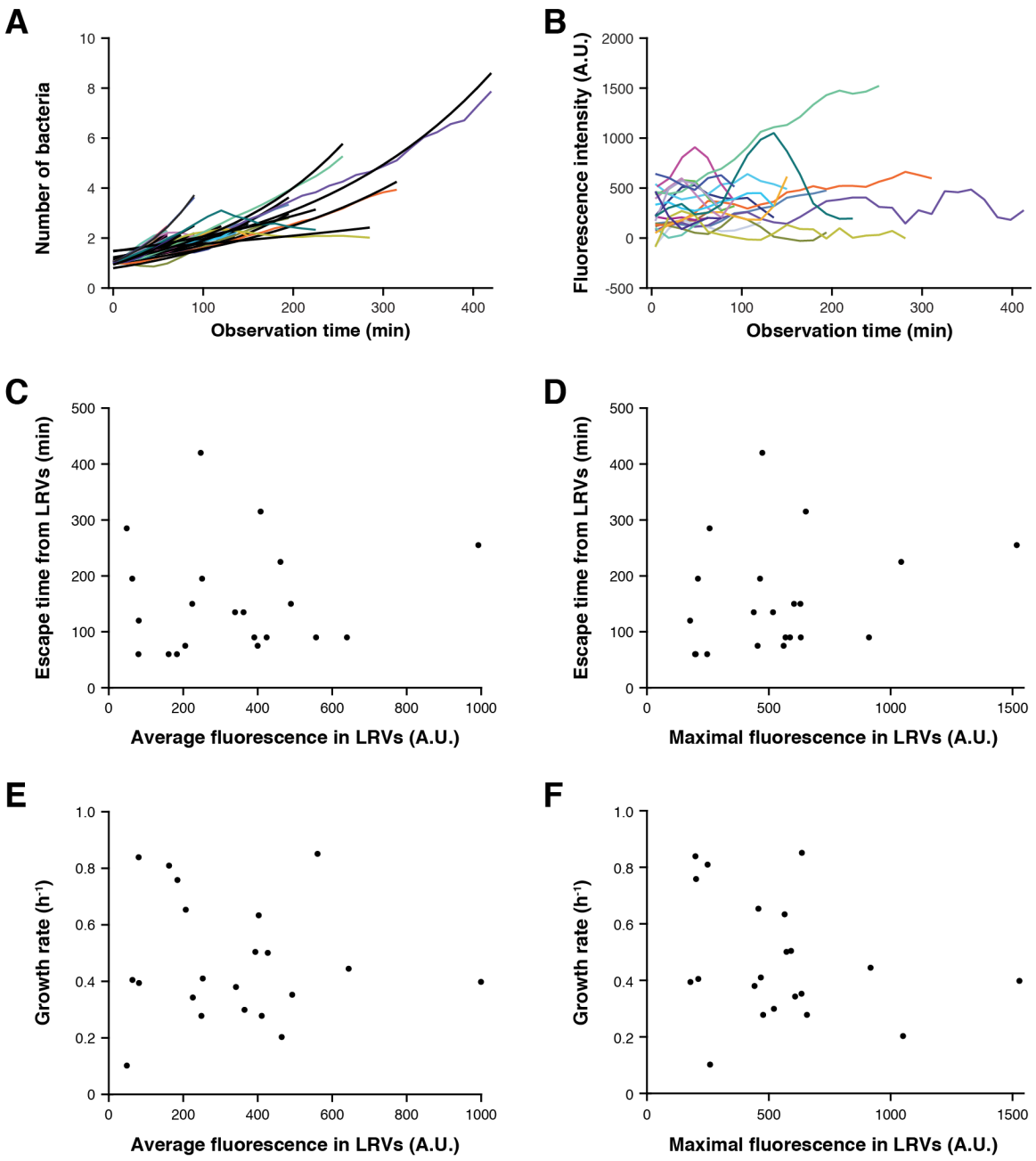

Figure S5. Quantitative and correlative analysis of the growth of bacteria and the secretion of LLO-FAST in LRVs over time.

LoVo cells were infected with *Lm* carrying an integrated pHpPL3-mCherry plasmid, and secreting FAST-LLO due to an in-frame C-terminal fusion with FAST as a *hlyA* locus.

(**A**) Number of bacteria and fluorescence of LLO-FAST inside LRVs over time. mCherry signals allowed the segmentation of bacteria and their counting over time.

(**B**) Quantification of the fluorescence over time in the FAST channel, which reports for the concentration of LLO-FAST in LRVs.

(**C**-**F**) Correlation between the fluorescence generated by LLO-FAST in LRVs and either the time of bacterial escape from, or the growth rate in, these compartments. The average intensity of fluorescence generated by the secretion of LLO-FAST (**C, E**) and the maximum intensity of LLO-FAST fluorescence (**D, F**) were extracted for each LRV (n = 21), and correlated with the duration of this compartment from the beginning of acquisition until membrane rupture (**A, B**) or with the growth rate of bacteria in this compartment, defined by the rate of increase of the size of the mCherry-labelled volume occupied by intravacuolar bacteria (**C, D**).

Supplementary Tables

Table S1. Bacterial strains

Strain	Description	Reference
LL195	*L. monocytogenes* LL195	(Weinmaier *et al*., 2013)
BUG1600	*L. monocytogenes* EGD-e	(Glaser *et al*., 2001)
BUG2479	*E. coli* DH5α [pAD-*cGFP*]	(Balestrino *et al*., 2010)
AG87	*E. coli* Rosetta(DE3)pLysS [pET28a-*FAST*]	(Plamont *et al*., 2016)
FXCV1	*E. coli* DH5α [pSU2.1rp-*mCherry*]	(Campbell-Valois *et al*., 2015)
JDS1	*E. coli* SM10 [pHpPL3-*mCherry*]	(Vincent *et al*., 2016)
M90T	*S. flexneri* M90T	(Sansonetti *et al*., 1982)
SF622	*S. flexneri* M90T Δ*ipaD*	(Ménard *et al*., 1993)
BIRD8	*E. coli* NEB5α [pAD-*SP-FAST-Myc*][†]	This work
BIRD9	*E. coli* NEB5α [pAD-*hlyA-Myc*]	This work
BIRD13	*L. monocytogenes* LL195 [pAD-*SP-FAST-Myc*]	This work
BIRD14	*L. monocytogenes* LL195 [pAD-*hlyA-Myc*]	This work
BIRD15	*E. coli* NEB5α [pAD-*FAST*]	This work
BIRD16	*L. monocytogenes* LL195 [pAD-*FAST-Myc*]	This work
BIRD17	*E. coli* NEB5α [pAD-*eGFP-Myc*]	This work
BIRD18	*L. monocytogenes* LL195 [pAD-*eGFP-Myc*]	This work
BIRD19	*E. coli* NEB5α [pAD-*SP-eGFP-Myc*]	This work
BIRD20	*L. monocytogenes* LL195 [pAD-*SP-eGFP-Myc*]	This work
BIRD32	*E. coli* NEB5α [pAD-*hlyA-FAST-Myc*]	This work
BIRD33	*E. coli* NEB5α [pAD-*hlyA-eGFP-Myc*]	This work
BIRD38	*L. monocytogenes* LL195 [pAD-*hlyA*-FAST-Myc]	This work
BIRD39	*L. monocytogenes* LL195 [pAD-*hlyA*-eGFP-Myc]	This work
BIRD62	*E. coli* NEB5α [pSU2.1rp-*ospF-FAST-Myc*]	This work
BIRD64	*E. coli* NEB5α [pSU2.1rp-*ipaB-FAST-Myc*]	This work
BIRD62	*E. coli* NEB5α [pSU2.1rp-*ospF-FAST-Myc*]	This work
BIRD64	*E. coli* NEB5α [pSU2.1rp-*ipaB-FAST-Myc*]	This work
BIRD66	*S. flexneri* M90T [pSU2.1rp-*ospF-FAST-Myc*]	This work
BIRD67	*S. flexneri* M90T [pSU2.1rp-*ipaB-FAST-Myc*]	This work
BIRD84	*S. flexneri* M90T Δ*ipaD* [pSU2.1rp-*ospF-FAST-Myc*]	This work
BIRD85	*S. flexneri M90T* Δ*ipaD* [pSU2.1rp-*ipaB-FAST-Myc*]	This work
BIRD127	*L. monocytogenes* LL195 Δ*hlyA*	This work
BIRD204	*E. coli* NEB5α [pMAD-*hlyA-FAST-Myc*]	This work
BIRD207	*L. monocytogenes* EGD-e *hlyA-FAST-Myc*	This work
BIRD213	*E. coli* NEB5α [pMAD-Δ*hlyA*::*SP-FAST-Myc*]	This work
BIRD217	*L. monocytogenes* LL195 [pHpPL3-*mCherry*]	This work
BIRD220	*L. monocytogenes* EGD-e *hlyA-FAST-Myc* [pHpPL3-*mCherry*]	This work
BIRD234	*L. monocytogenes* LL195 *prfA**	This work
BIRD240	*L. monocytogenes* LL195 *hlyA-FAST-Myc*	This work
BIRD244	*L. monocytogenes* LL195 *hlyA-FAST-Myc* [pHpPL3-*mCherry*]	This work

[†] All pAD constructs contain the P_{HYPER} constitutive promoter, the 5'-UTR of the *hlyA* gene, and the desired fusion protein. To simplify reading, the C-terminal Myc tag of constructs is not included in the plasmid names in the main text.

BIRD250	*L. monocytogenes* LL195 Δ*hlyA* [pHpPL3-*mCherry*]	This work
BIRD251	*L. monocytogenes* LL195 *prfA** [pHpPL3-*mCherry*]	This work
BIRD252	*L. monocytogenes* LL195 Δ*hlyA*::*SP-FAST-Myc* [pHpPL3-*mCherry*]	This work
BIRD256	*L. monocytogenes* LL195 Δ*hlyA* [pAD-*FAST-Myc*]	This work
BIRD257	*L. monocytogenes* LL195 Δ*hlyA* [pAD-*SP-FAST-Myc*]	This work
BIRD258	*L. monocytogenes* LL195 Δ*hlyA* [pAD-*hlyA-FAST-Myc*]	This work
BIRD259	*L. monocytogenes* LL195 Δ*hlyA* [pAD-*eGFP-Myc*]	This work
BIRD260	*L. monocytogenes* LL195 Δ*hlyA* [pAD-*SP-eGFP-Myc*]	This work
BIRD261	*L. monocytogenes* LL195 Δ*hlyA* [pAD-*hlyA-eGFP-Myc*]	This work
BIRD262	*L. monocytogenes* LL195 Δ*hlyA* [pAD-*hlyA-Myc*]	This work

Table S2. Oligonucleotides

Name	Description	Sequence	Ref.
oAL543	*Eag*I-UTR$_{hlyA}$ fw	tgtgtCGGCCGataaagcaa	This work
oAL544	*Xho*I-*Sal*I-Myc rv	CCctcgagGTCGACTTAtaa	This work
oAL545	FAST-UTR$_{hlyA}$ rv[‡]	acatgttcCATGGGTTTCACTCTCCTTC	This work
oAL546	UTR$_{hlyA}$-FAST fw	tgaaacccATGGAACATGTTGCTTTCGG	This work
oAL547	Myc-GFP rv	atttttgttcTTTGTATAGTTCATCCATGCC	This work
oAL548	GFP-Myc fw	actatacaaaGAACAAAAATTAATCTCTGAA	This work
oAL549	*Eag*I-UTR$_{hlyA}$ fw	gtgtgtCGGCCGataaagcaagcatataatattgcg	This work
oAL550b	*Sal*I-Myc-LLO rv	cgagGTCGACTTAtaaatcttcttcagagattaatttttgTTCGAT TGGATTATCTACTT	This work
oAL551b	FAST-LLO rv	gcaacaTGTTCGATTGGATTATCTACTTTAT	This work
oAL552b	LLO-FAST fw	ataatccaatcGAACATGTTGCTTTCGGTTC	This work
oAL553	GFP-SP$_{hlyA}$ rv[§]	ctcctttactATCCTTTGCTTCAGTTTGTTG	This work
oAL554	SP$_{hlyA}$-GFP fw	gcaaaggatAGTAAAGGAGAAGAACTTTTC	This work
oAL651	LLO-GFP rv	TCTCCTTTACTatgttcGATTGGATTATCTAC	This work
oAL652	GFP-LLO fw	CAATCgaacatAGTAAAGGAGAAGAACTTTTC	This work
oAL703	*Kpn*I-*ipaB* fw	ctcGGTACCaaggagtaattattATGCAT	This work
oAL704	*Bam*HI-*ipaB* rv	CATGTTCggatccAGCAGTAGTTTGTTGCAAAAT	This work
oAL705	OspF-*Bam*HI-FAST fw	GATAGAGggatccGAACATGTTGCGTTCGGCAG	This work
oAL706	*Xba*I-Myc rv	cgactctagaTTAcagatcttcctcagaga	This work
oAL707	*Kpn*I-OspF fw	ctcGGTACCagaggacgttttctATGCCC	This work
oAL708	*Bam*HI-OspF rv	TTCggatccCTCTATCATCAAACGATAAAAT	This work
oAL974	*Sal*I-*hlyA* fw	TCCATATGACgtcgacAGCATTTAAAGCTGTA	This work
oAL975	3' of *hlyA*-Myc rv	ttacttttacaaTTAtaaatcttcttcgctga	This work
oAL976	Myc-3' of *hlyA* fw	gaagatttaTAAttgtaaaagtaataaaaaattaag	This work
oAL977	*Bgl*II-*mpl* rv	TTAACTAGACagatctTTGTGGGTATCAGC	This work
oAL981	*Sal*I-*plcA* fw	TCCATATGACgtcgacACTCGGACCATTGTAG	This work
oAL984	FAST-SP$_{hlyA}$ rv	aaagcaacatgttcATCCTTTGCTTCAGTTTG	This work
oAL985	SP$_{hlyA}$-FAST fw	ggatGAACATGTTGCTTTCG	This work

[‡] UTR$_{hlyA}$ refers to the 5'-UTR of the *hlyA* gene, bringing a ribosome binding site (RBS) and used to enhance gene expression (Shen and Higgins, 2005).

[§] SP$_{hlyA}$ indicates to the sequence encoding the signal peptide from LLO (*hlyA* gene).

fw, forward strand; rv, reverse strand.